Materials & Design 237 (2024) 112552

Contents lists available at ScienceDirect

Materials & Design

journal homepage: www.elsevier.com/locate/matdes

Modelling and experimental study of laser-assisted milling of fibre reinforced SiC/Ti-6Al-4V metal matrix composite

Omkar Mypati, Jeriel Panzer, Jose A. Robles-Linares, Shusong Zan, Zhirong Liao *, Dragos Axinte

Machining and Condition Monitoring Group, Faculty of Engineering, University of Nottingham, NG8 1BB, United Kingdom

ARTICLE INFO

Keywords:
Laser-assisted machining
Metal matrix composites (MMCs)
Ti6Al4V
SiC fibre
Tool wear
Surface integrity

ABSTRACT

Metal matrix composites (MMCs) offer unique advantageous mechanical properties by strengthening a ductile metal matrix with a ceramic reinforcement (e.g., Ti6Al-4 V/SiC_f). However, their heterogeneous composition poses machining challenges including fibre pullout, matrix cracking, and increased tool wear. Whilst pre-heating via laser-assisted machining (LAM) shows promise for improving machinability, traditional LAM implementations with a fixed laser spot size and straight laser path prevent uniform heating. By introducing spatially and temporally controlled LAM that generates homogeneous heating by varying the laser scanning velocity, a technique called fully inverse LAM can be applied for MMCs. This involves calculating separate temperature fields for the matrix and reinforcement to minimise thermal mismatch stresses. The fully inverse LAM decreases subsurface cracks and delamination resulting from conventional milling, whilst localised matrix softening reduces cutting forces by over 62 %. Flank tool wear is also diminished, increasing tool life by 120 %. Material analysis reveals reduced machined surface damage, lower surface roughness, and less formation of intermetallic compounds (Ti_2C) compared to traditional LAM.

1. Introduction

Metal matrix composites (MMCs) have emerged as advanced materials for structural applications where high specific strength and stiffness are critical performance requirements. Because of their superior mechanical properties, including high strength, stiffness, wear resistance, and lightweight nature, MMCs have gained increasing attention in high-performance applications such as in the aerospace and automotive fields [1,2]. The machining of MMCs presents challenges due to the interaction between the metal matrix like Al, Ti, Mg or Cu and ceramic reinforcements like particles (SiC, Al_2O_3, TiO_2, CNT, TiC and graphene etc.) and fibres (SiC, C, etc.). Among these, carbon-based reinforcements improve the composite's properties (e.g., thermal conductivity and coefficient of thermal expansion) [1]. Yield strength, wear resistance and other mechanical performance indicators of the MMC are improved by TiC particles, SiC fibres (SiC_f) and SiC particles and W fibres, respectively [1].

During the machining of particle-reinforced MMC, the differences in mechanical properties between the metal matrix and reinforced particles lead to localised stress concentrations and deformation [3]. The matrix's lower elastic modulus and higher ductility to plastic strains concentrate around the stiffer, brittle particles [4]. Specifically, the rigid reinforced particles serve as stress risers that amplify strains in the more compliant metal matrix. This strain amplification results in the matrix yielding plastically due to the localised triaxial stresses exceeding the matrix yield strength. Consequently, microscopic voids and cracks initiate near the particle–matrix interfaces [5,6]. In addition to plastic deformation, the mismatch in the coefficient of thermal expansion between the particle and matrix phases promotes microcracking. During cooling after machining, the more significant contraction of the metallic matrix compared to the particles induces thermoelastic stresses along the interfaces. These residual stresses build up in the matrix, which can lead to debonding and microcracking at the particles. Further, any fractured or broken particles act as sharp stress concentrators that readily initiate cracks in the surrounding matrix [7,8]. As shown in Fig. 1(a), these cracks emanate from the fractured particles and spread by linking with neighbouring voids and defects. The combined effects of concentrated plastic flow, mismatch stresses, and fractured particle stress risers result in extensive microcracking within the matrix phase. These cracks reduce the effective load-bearing area, serving as sites for

* Corresponding author.
E-mail address: Zhirong.Liao@nottingham.ac.uk (Z. Liao).

https://doi.org/10.1016/j.matdes.2023.112552
Received 23 October 2023; Received in revised form 4 December 2023; Accepted 4 December 2023
Available online 10 December 2023

additional crack formation and growth when external stresses are applied. While particle reinforcement can increase mechanical properties, discrete particles are less effective at hindering crack propagation than continuous fibre reinforcement [9].

Unlike particle reinforced MMCs, the long continuous fibres in MMCs can be aligned in particular directions, imparting strength and enabling the material to withstand higher stresses [10,11]. This anisotropic orientation makes fibre-reinforced composites as "advanced" MMCs compared to more isotropic particle-reinforced MMCs. Machining of carbon fibre-reinforced plastic (CFRP) and fibre reinforced MMCs shows great variation in understanding the cutting forces and tool wear. However, the machining of both CFRPs and MMCs leads to surface and subsurface defects that deteriorate the mechanical performance of the industrial components. Defects in CFRPs include fibre pullout, delamination, thermal damage, and surface cavities [12]. Fiber reinforced MMCs also exhibit fibre pullout and debonding, along with plastically deformed surface layers and subsurface microcracks from concentrated shear stresses during cutting, as shown in Fig. 1(b) [9,13]. The metallic matrix experiences more significant subsurface plastic deformation compared to the polymer matrix of CFRPs. However, the differing properties between the ceramic fibre and metal matrix in MMCs intensify thermal mismatch stresses and incompatible deformation during machining. The variance in strength and stiffness between the reinforcing fibres and surrounding metal matrix can cause incompatible deformation and interfacial debonding at the fibre–matrix interface. Specifically, the ductile matrix undergoes substantial plastic deformation and grain refinement in the subsurface shear zones during MMC machining [14]. Further, it also undergoes matrix grain refinement from concentrated shear stresses beneath the machined surface due to the interrupted load transfer between the tool and the stiffer reinforcing fibres along the tool path. This localised interface deformation could reduce the load transfer efficiency between the two phases, compromising the overall strength and performance of the composite [9]. Furthermore, fibres aligned perpendicular to the cutting direction undergo brittle fracture and fragmentation during machining instead of shearing plastically like the matrix phase [15]. All of these aspects are characteristics of machining fibre-reinforced MMCs, highlighting the challenges that need to improve surface integrity towards the functional performance of MMC components [16].

As mentioned, fibre reinforced MMCs offer an exceptional combination of properties uniquely suited to aerospace components. In aerospace engines, incorporating fibres exhibits excellent dimensional stability under fluctuating temperatures due to their high stiffness and low coefficient of thermal expansion [11]. However, most of the existing literature focuses on processing methods and characterising mechanical performance. In one study, K.M. Rahman et al. [17] worked on high-strength Ti-SiC composites using a Ti-5Al-5Mo-5 V-3Cr matrix reinforced with unidirectional SiC_f. Due to its anisotropic mechanical properties, the composite exhibited impressive tensile and compressive strengths exceeding 2GPa and 3.5GPa. The fatigue behaviour of a similar Ti-SiC composite with TC17 titanium alloy reinforced with unidirectional SiC_f was studied by Y. Wang et al. [18]. A fatigue stress amplitude was tested, leading to fibre fractures and unstable rapid crack growth. Still, there is a need to further study the machinability behaviour of these long fibre-reinforced MMCs. In line with this need, Zan et al. [15] investigated the fundamental cutting mechanisms of $Ti6Al4V/SiC_f$ MMCs through orthogonal cutting experiments performed perpendicular to the fibre direction at controlled temperatures of 400 °C, room temperature, and −180 °C. They observed cracking in SiC fibres below the machined surface resulting from bending forces during machining. The study revealed that temperature strongly influences material removal in MMCs by altering matrix properties when interacting with fibres. While providing details on cutting physics of long-fibre MMCs and highlighting temperature-dependent matrix deformation, the fundamentals of milling long-fibre MMCs remain poorly comprehended. Further research is still required to elucidate relationships between microstructure, cutting parameters, and machining-induced damage in order to advance the milling process for these highly heterogeneous composites ($Ti6Al4V/SiC_f$).

The hard, abrasive reinforcement fibres such as SiC in these MMCs make the cutting tools prone to accelerated wear during the machining of these composites. As the cutting tool shears through the composite, exposed fibres act as abrasives and increase wear rates [19]. A higher fibre volume fraction in the MMCs leads to more abrasion and faster tool wear. Among the primary wear modes is flank wear on the clearance face of the tool caused by fibre rubbing and crater wear on the rake face caused by direct contact with the cut fibres in the chip [20]. In addition, fractured fibres during machining create sharp new edges on the broken fragments, intensifying the tool's surface abrasion [21]. Additionally, abrasive fibres increase thrust forces during machining. As a result, tool wear is further intensified [22]. When machining MMCs, cement carbide tools wear out quickly due to harder reinforcement. Polycrystalline diamond (PCD) and cubic boron nitride (CBN) inserts provide superior tool wear resistance to carbide inserts [23,24]. For machining most of the MMCs, PCD exhibits the best performance due to its higher Vickers hardness and superior thermal conductivity than CBN [23,25]. PCD is chemically inert while machining MMCs, while CBN can react with some matrix alloys at high temperatures [26]. PCD inserts are generally preferred for milling most MMCs due to superior abrasive and thermal wear properties [24]. However, the highly heterogeneous material used in this study exhibits high tool wear and deteriorated surface quality when machined at high cutting speeds and feeds. Preheating these difficult-to-cut MMCs with heat sources like lasers or induction heating systems prior to cutting can enable more aggressive milling parameters

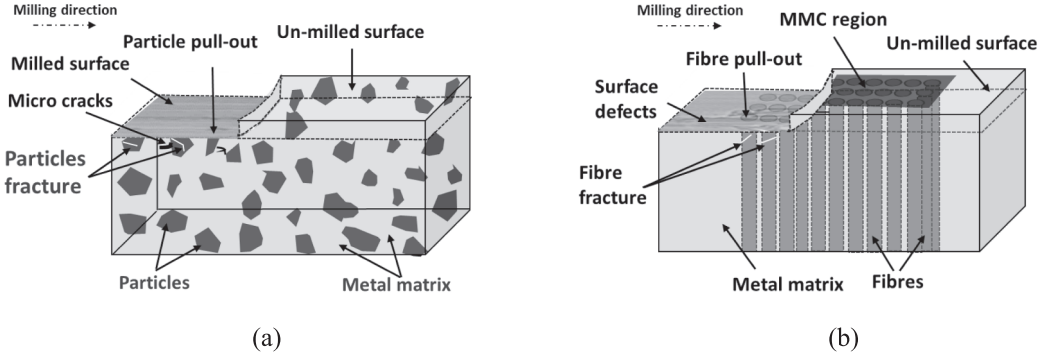

Fig. 1. Schematic of usual industrial grade MMCs and their associated machining-induced defects. (a) Particle-reinforced MMC with randomly distributed ceramic particles embedded in a metal matrix. The machined surface has typical defects like micro-cracks, particle pullouts and fractured embedded particles. (b) Fibre-reinforced MMC with continuous ceramic fibres aligned unidirectionally in a metal matrix. The machined surface highlights defects like fibre pullouts, fractures, and surface cavities.

without sacrificing tool life or surface finish. Of these two heating sources, laser-assisted machining (LAM) has shown feasibility for improving the machinability of these challenging MMCs [27–29].

However, implementing LAM on these highly heterogeneous MMCs is challenging. In traditional LAM, the laser spot size is much smaller than the sample width, as shown in Fig. 2(a). This can lead to non-uniform heating outside the laser spot area over the MMC surface, where the SiC fibres absorb more heat while the Ti matrix does not soften properly [30,31]. While machining, these unevenly heated MMCs may cause more surface and subsurface damage. Recently, Shang et al. [30] developed a novel spatially and temporally controlled laser heating approach called inverse modelling. This enables homogeneous heating on surface areas much larger than the laser spot size by oscillating the laser with varying velocities or scanning paths (see Fig. 2(b)). The optimal laser parameters are derived by solving equations of coupled thermal forward and inverse problems. The forward analysis predicts the temperature field for defined laser conditions, while the inverse analysis determines the required power and velocity to achieve the target temperature distribution. However, Shang et al.'s inverse model approach is feasible for homogeneous materials, where optimal scanning paths are obtained by considering a single material's properties. As shown in Fig. 2(c), the complexity of implementing the inverse problem model on MMC materials can be explained as follows: This specific MMC material is intentionally designed with SiC fibres for aerospace components. The upper and lower sections comprise a Ti metal matrix, while the middle section where the fibre reinforcement is located sits at the exact centre. A major challenge in machining this MMC using the inverse model is the presence of the central fibre-reinforced section, which makes the MMC highly heterogeneous. In the Ti6Al4V/SiC_f MMCs, this heterogeneity causes the titanium matrix to rapidly absorb laser energy and heat up. However, the SiC fibres have lower absorption and high conductivity, resulting in uneven temperature gradients across the material. Due to this thermal mismatch between the matrix and reinforcement, the heat absorption will be different when applying the traditional inverse model to the MMC. Hence, advanced multi-physics simulations are needed to model the complex interactions between the laser, matrix and fibres in this heterogeneous composite. A multi-layer approach defining the properties of each phase enables physics-based prediction of optimal laser scanning velocities (see Section 2.2.2). In addition to confirming the potential of the inverse model for process enhancement, more work is needed to understand the fundamental mechanisms when machining this composite. A detailed analysis of force variation, tool wear, chip formation, surface integrity and subsurface damage is also required, comparing traditional and modified inverse problem LAM methods. This analysis will provide further insight into the advantages of implementing inverse modelling for machining these difficult-to-cut, highly heterogeneous MMCs. Moreover, the milling mechanics for the Ti6Al4V/SiC_f MMCs have not yet been studied by any researcher.

2. Development of a mathematical model for heterogeneous MMC materials

2.1. Novel inverse model for highly heterogeneous MMCs

In the traditional LAM process, the laser spot is continuously focused on a specific location to heat the material (see Fig. 2(a)), followed by the milling operation [32,33]. However, the heat distribution is not homogeneous with this traditional approach. In this regard, Z. Shang et al. [30] proposed a novel inverse model to achieve uniform heat distribution across the sample width for homogeneous materials (Inconel 718). However, given the heterogeneity of MMCs, directly applying the model of Z. Shang et al. is not technically feasible (referred to as semi-inverse LAM here). In order to observe the fidelity of the inverse model, preliminary trials with different laser powers were validated by incorporating thermocouples on the top surface and at 0.2 mm depth along the thickness direction. The results showed a 5–7 % deviation from the peak temperature predictions. The novelty of the current model arises through the addition of varying laser scanning velocities along defined paths for specified material regions (referred to as fully inverse LAM). This modification aims to improve the inverse model by accounting for heterogeneity, enhancing its applicability for this MMC composite. The fundamental mathematical equations required to establish the Gaussian

Table 1
Non-homogeneous Ti6Al4V/SiC_f MMC material properties [15].

Property	Ti6Al4V	SiC
Density (Kg/m^3)	4430	3100
Melting point ($^\circ C$)	1604–1660	2730
Specific heat capacity ($J/kg/K$)	526.3	670
Thermal conductivity ($W/m/K$)	6.7	77.5

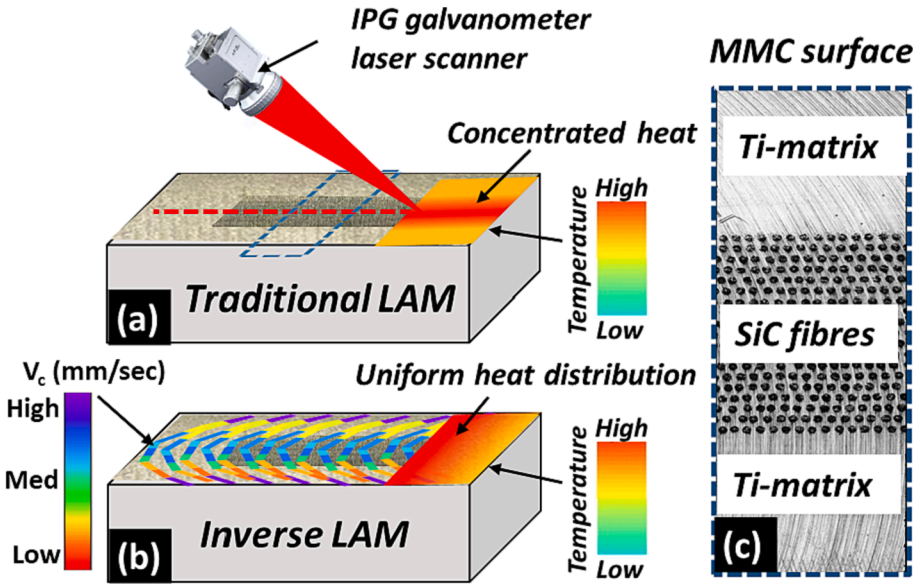

Fig. 2. Schematic of representation of laser scanning path and corresponding heat distribution (a) traditional LAM, (b) inverse model LAM and (c) heterogeneous MMC material surface.

beam model based on user-defined material properties (see Table 1), which are essential for developing the inverse model, are provided in Appendix 1.

2.2. Implementing traditional inverse problem (semi-inverse LAM) on heterogeneous MMCs

The previously developed semi-inverse LAM technique for homogeneous materials is implemented here for heterogeneous MMCs (Fig. 3a), in order to identify its capabilities for these composites. This semi-inverse approach applies arithmetic averaged properties of the Ti and SiC phases (see Eq.(1)), with Neumann boundary conditions modelling semi-infinite conduction [34,35]. However, the inverse model is performed to obtain a temperature of 650 °C at 0.2 mm below the top surface. A temperature of 650 °C is just below the β-transus range of 700–1050 °C for Ti6Al4V alloy [36]. Exceeding the β-transus during laser-assisted machining risks grain growth and other microstructural changes in the titanium alloy that negatively impact mechanical properties [36,37]. Thus, the inverse model optimises the localised laser heating to keep peak temperatures right at this critical threshold of 650 °C. This heating level is sufficient to getter meaningful thermal softening benefits for enhanced machinability, including reduced cutting forces and tool wear. Simultaneously, confining heating to just below the β-transus range preserves favourable phase distributions and fine grain sizes following processing. In essence, through physics-based modelling of the Ti6Al4V thermal response, the model optimises the laser scanning velocity based on the mean properties (i.e., averaged properties across the whole surface), thus enabling uniform heating across the whole material, as shown in Fig. 3(a,c). However, this results in non-unfirm temperature, and causes over-softening of the Ti matrix, leading to disadvantages in cutting forces variation, tool wear, and subsurface integrity. Therefore, while providing initial insights, this semi-inverse technique has limitations for heterogeneous materials. Hence, it represents an intermediate step before developing the comprehensive fully inverse model, which accounts for heterogeneity and optimises the LAM process parameters specifically for MMCs.

$$\theta(x,y,z,t)_{Semi-inverse} = \frac{1}{2}[\theta(x,y,z,t)]_{Ti} + [\theta(x,y,z,t)]_{SiC} \quad (1)$$

2.3. Suitable laser scanning method (Fully inverse LAM) for highly heterogenous MMCs

The main difference between the semi-inverse technique and a fully inverse model is incorporating the distinct thermal and material properties of the Ti matrix and SiC_f reinforced regions. Due to the heterogeneous material composition, varying the laser scan velocity in different regions is necessary. Due to the higher thermal conductivity of the SiC_f, the laser scan velocity needs to be lower in the SiC_f reinforced region in order to sufficiently soften the fibres as compared to the Ti region. In contrast, laser scanning should be faster in the Ti region to mitigate thermal failure in the metal matrix composite (see Fig. 3 (a,b)). Hence, based on the different thermal conductivities, densities, and heat capacities of Ti and SiC, the governing heat transfer equations would model the transient temperature field in the Ti-SiC regions by stitching the material properties in the heat generation equations (Eq. 2). Further, the cost function is optimised with $\theta(x,y,z,t)_{fullyinverse}$ fully inverse to obtain varying velocities along the predefined path.

$$\theta(x,y,z,t)_{fullyinverse} = [\theta(x,y,z,t)]_{Ti} + [\theta(x,y,z,t)]_{SiC} \quad (2)$$

where, $[\theta(x,y,z,t)]_{SiC}$ is zero when considering the Ti-matrix region and $[\theta(x,y,z,t)]_{Ti}$ is zero when considering the SiC reinforcement region.

Hence, based on the varied material properties, the scanning velocities differ along the path as shown in Fig. 3(b). This model can generate optimal laser scan trajectories by numerically optimising velocity profiles along predefined paths to generate the heat distribution across the sample width as shown in Fig. 3(c). In regions with low laser absorption and high thermal conductivity and heat capacity (i.e., the SiC fibre regions), the laser scan velocity will be decreased to soften the SiC fibres. In contrast, the velocity will be higher in the Ti matrix regions to prevent overheating. Implementing a fully inverse modelling approach accounts for these heterogeneous properties. This enables tailored regional scan

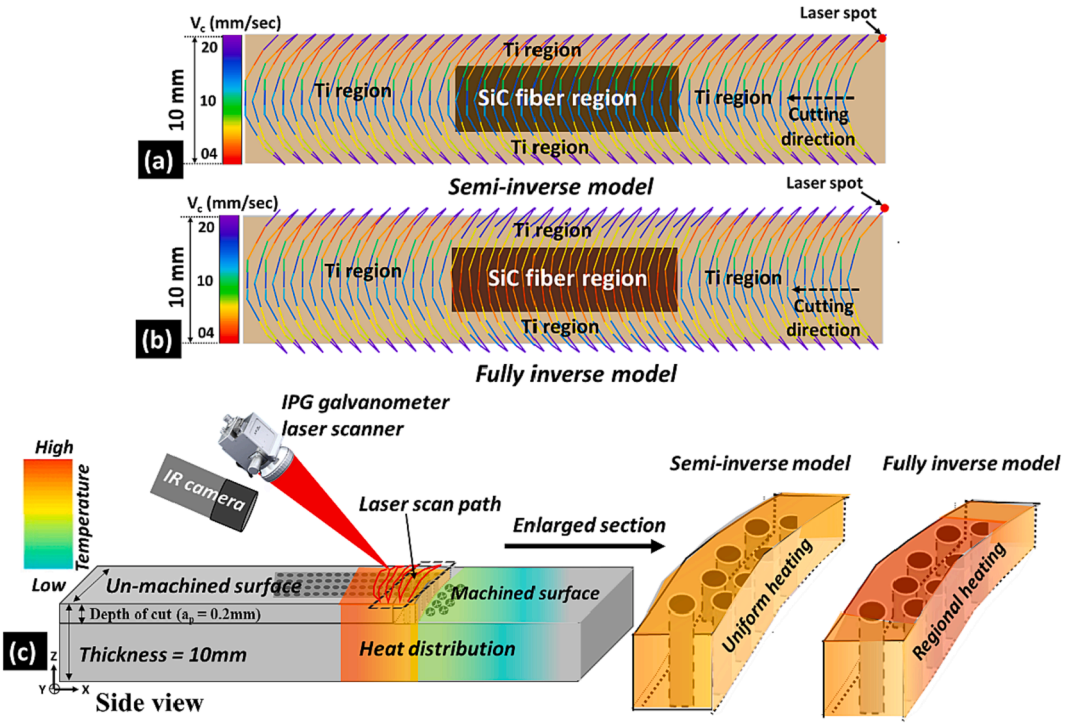

Fig. 3. Schematic of the implementation of (a) semi-inverse and (b) fully inverse LAM of Ti6Al4V/SiC_f MMC: (c) optimised laser scanning paths based on velocity and heat distribution in heterogenous MMCs.

velocities which reduce material damage compared to current semi-inverse methods. Additionally, minimising the cost function during velocity optimisation can target deviations from the desired temperature profile in both the matrix and reinforcement regions simultaneously. Hence, a multi-material inverse problem approach is developed and implemented in-house for machining trials. Mainly, the model executes based on the provided material properties, generating an output DXF file with the laser path with varying velocities. Consequently, the customised multiphase velocity profile significantly improves the heating mechanism according to the material properties and machining performance, thereby providing non-uniform heating, but uniform temperature.

3. Understanding the machining of highly heterogenous MMCs

3.1. Details of heterogenous MMC material

The MMC material used in this research is with Ti6Al4V as the metal matrix and SiC_f as reinforcement with a fibre diameter of 140 μm, where the reinforcement region is located in the middle of the sample as shown in Fig. 4(a). This special material was produced by TISICS Metal Composites, where the SiC_f is aligned along the thickness direction while maintaining uniform spacing between each fibre (see Fig. 4(b)). Furthermore, the alignment of fibres along the thickness direction (i.e., cross-sectional view) of the material provides information on the fibre–matrix bonding, as depicted in Fig. 4(c).

The as-received Ti6Al4V/SiC_f MMC exhibits a bimodal microstructure comprising equiaxed primary α-Ti phases and β-Ti phases within the Ti alloy matrix, as shown in Fig. 4(d). Combining the ductile Ti6Al4V matrix and high-stiffness SiC_f enables excellent specific mechanical properties that make Ti6Al4V/SiC_f MMCs a promising material for structural applications in aerospace engines [17]. The tailored multiphase microstructure balances strength, toughness, and creep resistance at reduced densities compared to monolithic Ti-alloys. Additionally, the high-temperature stability of the SiC_f imparts improved thermo-mechanical performance critical for engine components. With their superior specific properties, Ti6Al4V/SiC_f composites have significant potential to reduce weight and enhance efficiency in next-generation aerospace systems [11,17].

3.2. Inhouse experimental setup for the LAM trails

LAM trials were performed on Ti6Al4V/SiC_f MMC using a Tormach 1100 MX CNC milling machine integrated with a 2 kW fibre laser (IPG Photonics YLR 2000S). The laser was fitted with a galvanometric scanner having a 12 mm mirror clear aperture. An HLC-8 fibre adapter was used, and the scanning head tilted 45° to align the scanning path horizontally with the milling feed direction (see Fig. 5). The cutting speed and laser focus diameter were set to 100 m/min and 3 mm, respectively, with the laser positioned to scan the top surface to develop a uniform heat distribution of 650 °C at a depth of 0.2 mm in the MMC workpiece (Fig. 5). This temperature was selected to prevent the formation of dendritic phases in the Ti matrix. The cutting tool consisted of an R217.53–2025.3S-09-3A indexable carbide insert holder fitted with three PCD20 cutting edges (SEEX09T3AFFN-L1); all the cutting tools and inserts were provided by SECO Tools UK. A constant Cutting speed (v_c) of 100 m/min, 0.2 mm depth of cut (a_p) and 0.05 mm/tooth feed rate (a_f) were utilised, with the insert specifications and cutting parameters summarised in Table 2.

The 12° positive rake angle of the cutting insert was selected for a promoted chip flow, and its tendency to aid in minimising cutting forces during the milling of the MMC material by enabling easier shearing of the material and chip curling. Extensive benchmarking trials identified optimal machining parameters for analysing tool wear and cutting forces. A FLIR A325 infrared camera, which could measure temperatures from −20 °C to 2000 °C, was utilised to measure the surface temperature of the workpiece during machining. Numerous benchmarking tests with embedded workpiece thermocouples confirmed the fidelity of the surface temperature measured with the IR thermography camera; thus, a sampling rate of 25 Hz and an emissivity value of 0.65 were employed. A 3-axis dynamometer (Kistler 9257A) coupled with NI 9233 DAQ measured cutting forces up to 5 kN and 10 kN in the X/Y and Z directions, respectively (see Fig. 5). A sampling rate of 20 kHz allowed the characterisation of force fluctuations in the reinforcement region, which can be correlated to progressive tool wear by detecting localised microscale variations indicative of surface damage.

3.3. Material characterisation techniques to evaluate the various machining conditions for heterogeneous MMCs

Various material characterisation techniques were employed to comprehensively evaluate the effects of different machining processes on the Ti6Al4V/SiC_f MMC samples. Specifically, the, tool wear, chip morphology, microstructure and surface integrity, were analysed to determine the impacts of conventional versus laser assisted milling. After the machining trials on MMCs, the cutting inserts, the chip morphology and the machined surfaces were inspected under scanning electron microscopy (SEM: JEOL FEG-SEM 7000F and JEOL FEI Quanta 650 eSEM, respectively). To achieve this, the samples are polished up to 0.02 μm particle size colloidal silica, which also produced a sufficiently smooth surface quality for electron back scattered diffraction (EBSD) using JEOL FEG-SEM 7100F. The EBSD analysis is performed using a probe current of 12nA, accelerating voltage of 15 kV and a step size of 0.15 μm. Further, Kroll's reagent (Distilled water 92 ml, Nitric acid 6 ml, and Hydrofluoric acid 2 ml) was employed as etching agent to study the grain refinement for conventional milling and LAM of Ti6Al4V/SiC_f MMC. Additionally, the machined surfaces were analysed under an Alicona G4 to measure the surface roughness for different process

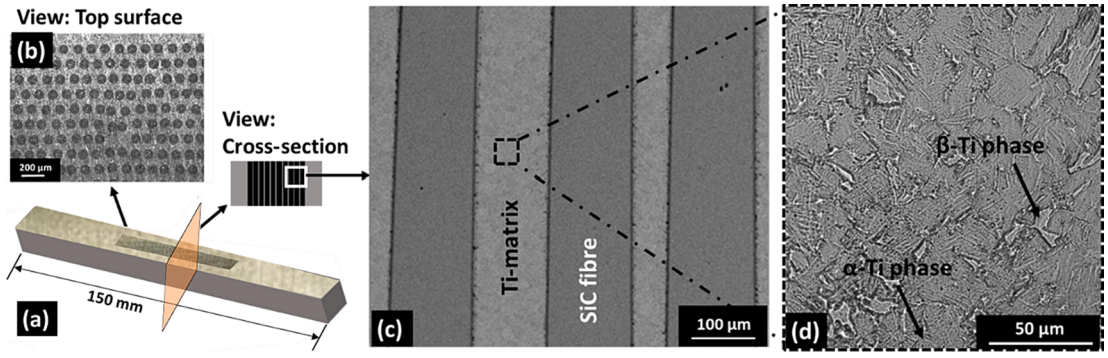

Fig. 4. (a) Ti6Al4V-SiC_f MMC, (b) top view in the reinforcement region to show the SiC_f locations, (c) cross-section view showing alignment of SiC_f, and (d) microstructure of as-received Ti-matrix with α-Ti, β-Ti phases.

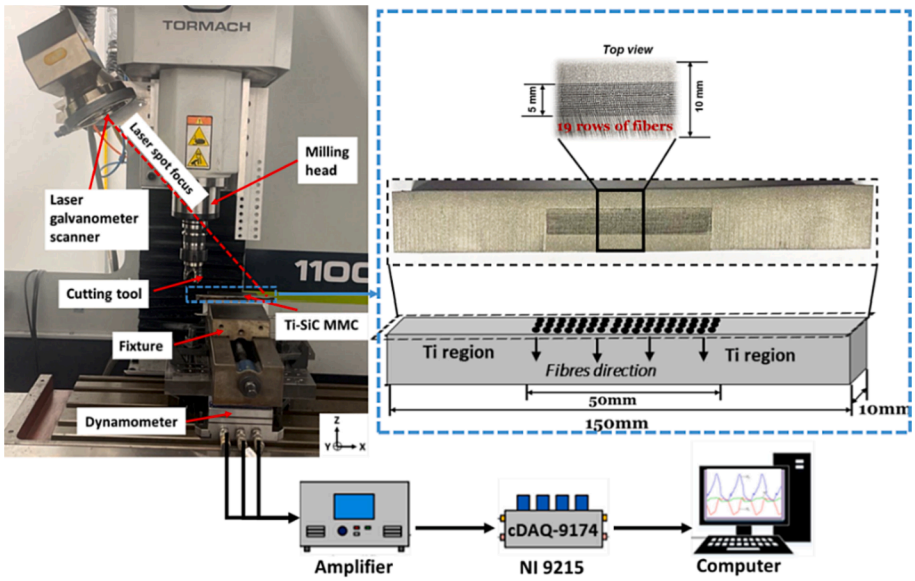

Fig. 5. Experimental setup schematic for the laser-assisted milling, showing temperature monitoring by thermal camera on the top surface and cutting force measurement by a multi-channel dynamometer. The laser spot is ahead of the cutting tool by 3 mm.

Table 2
Cutting parameters and tool insert specifications.

Cutting speed v_c (m/min)	Feed rate a_f (mm/tooth)	Depth of cut a_p (μm)	Clearance angle (°)	Rake angle (°)	Edge length (mm)	Corner radius (mm)	Cutting edge length (mm)
100	0.05	200	26	12	1.5	0.4	1.95

conditions. Furthermore, the machine cutting inserts were subjected to tool wear measurements using open-source image processing software (ImageJ) to determine the distance between the new tool flank face contour and the worn tool contour.

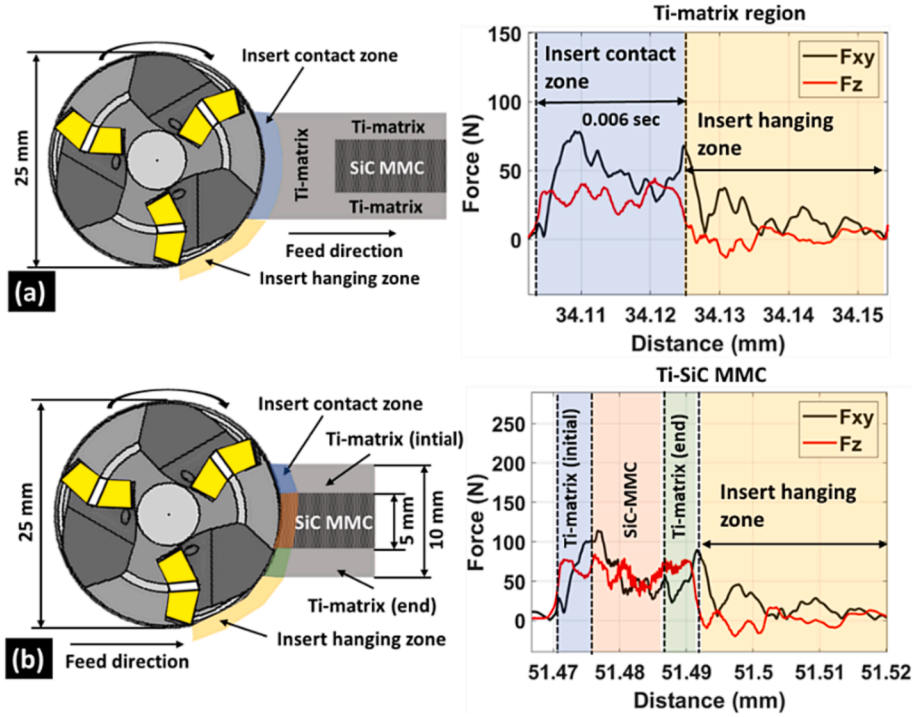

Fig. 6. Resultant and axial cutting forces at (a) initial Ti-matrix region and (b) Ti-SiC reinforced region.

4. Results and discussions

4.1. Reduced cutting forces with implementing fully inverse LAM for $Ti6Al4V/SiC_f$ MMC

Force analysis was performed in this study to quantify the reduction in cutting forces enabled by LAM for this heterogeneous composite. The cutting force measurements directly correlate to the reduced mechanical properties of the Ti-matrix phase owing to laser irradiation, providing insights into tool wear progression and chip morphology changes associated with the improved machinability [38]. Under different milling conditions (i.e., conventional, semi-inverse and fully inverse), measuring the time-varying cutting forces provides a critical understanding of milling efficiency and progressive tool wear. Based on the cutting parameters, the tool exhibits a 0.0164 s/rev spindle speed, and each tooth covers a 0.05 mm feed per revolution axially across the

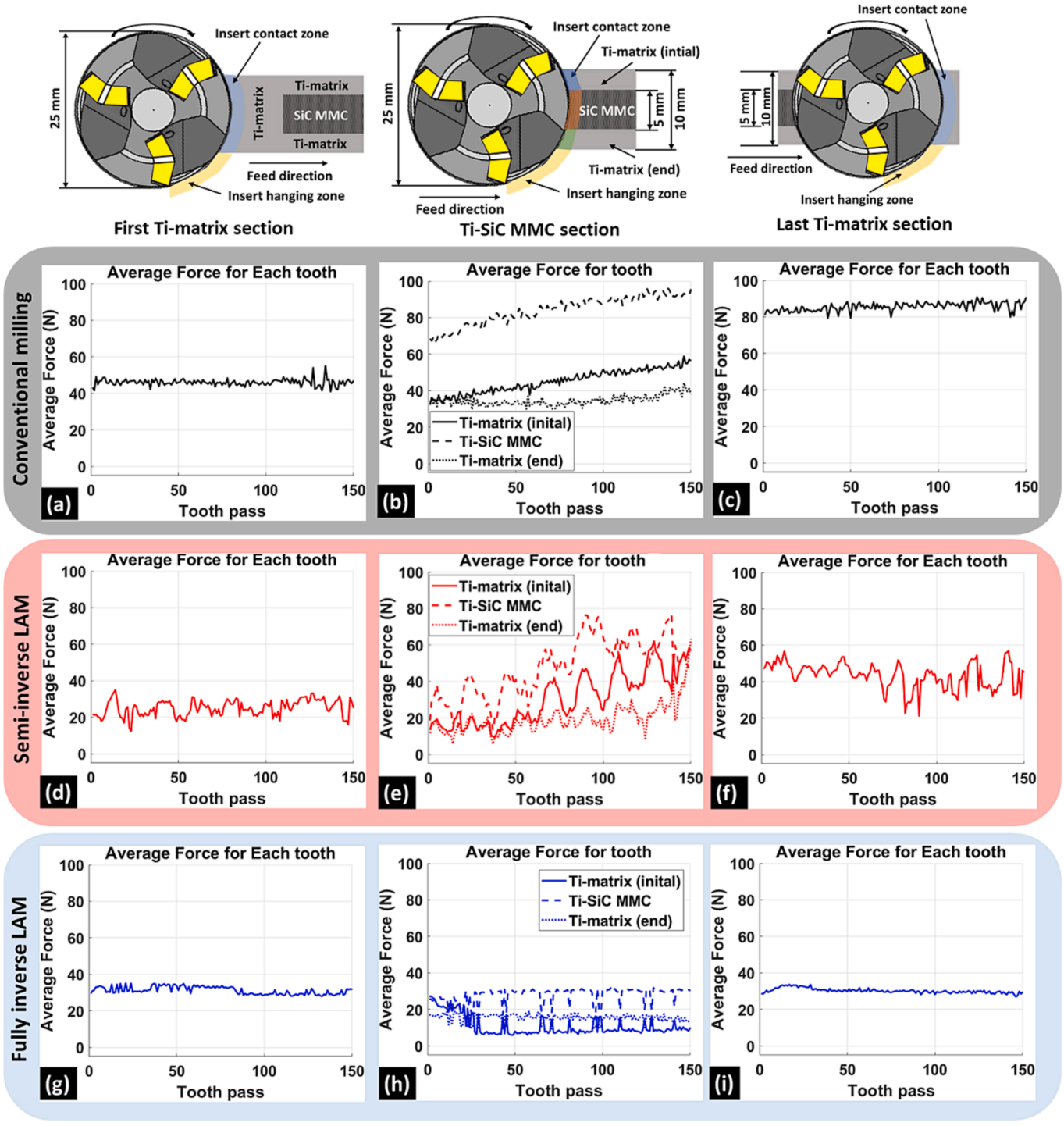

Fig. 7. Segmented cutting force response for individual tooth passes in discrete regions under different LAM strategies. Acquired forces in the (a,d,g) first Ti matrix section, (b,e,h) Ti-SiC reinforced MMC section, and (c,f,i) last Ti matrix section during milling under (a-c) conventional conditions, (d-f) semi-inverse LAM, and (g-i) fully inverse LAM. Segmenting the force response elucidates the distinct effects of the laser assistance strategies on the cutting mechanics in each material region. The data enables analysis of tool-workpiece interactions across the different sections.

workpiece length. However, a single insert is only in cutting contact over 0.006 s, traversing the 10 mm workpiece width, spending the remainder of the revolution in a non-cutting "hanging" region, as highlighted in Fig. 6(a,b).

Relating the measured forces to the tool location and engagement state provides insight into the distinct cutting phenomena governing material removal. In the schematic of cutting the sub-section of the Ti-matrix (initial) region, the resultant force is increased when the insert engages with the workpiece. After 0.006 s, the force decreases, indicating the tool hanging part. The cutting force behaviour in the SiC reinforced region looks different compared to the initial section (0.0015 s). The force increased when the cutting insert engaged with the reinforced region, which exhibited fluctuation in the next 0.003 s time, and the forces tended to decrease in the end section of the Ti-SiC reinforcement region, as depicted in Fig. 6(b). Based on this analysis, the average force along the three sub-sections in the reinforcement region can be measured, and the trends can be analysed to correlate with the tool wear.

The cutting force analysis, correlated to the tool position across the three distinct sections of the machined Ti6Al4V/SiC_f MMC, revealed varying force trends unique to each zone under the different machining conditions. In the initial Ti-matrix section, the average resultant cutting force per tooth pass remained relatively constant at 50 N, 25 N, and 35 N during conventional milling, semi-inverse LAM, and fully inverse LAM, respectively, as shown in Fig. 7(a,d,g), respectively. The minimal fluctuations of less than 5 N between each sequential tooth pass produced uniform minimal tool wear throughout the machining of this initial Ti zone for all cutting conditions. The reduced average force of approximately 25 N (-50 %) with semi-inverse LAM compared to 35 N (-30 %) with fully inverse LAM originates from differences in the localised laser power density and optimised scanning strategies affecting the thermal softening of the Ti matrix. Specifically, the approximately 10 N disparity arises between semi-inverse and fully inverse LAM is because the semi-inverse model incorporates average thermal-physical properties of the Ti and SiC phases. At the same time, the fully inverse approach exclusively considers the properties of the Ti matrix in simulating this initial region, leading to a higher predicted scan velocity which leads to lower heat generation. Upon entering the SiC-reinforced zone of the MMC, the forces in the Ti-matrix (initial) subsection remained comparable to the forces observed in the first Ti-matrix section. However, as shown in Fig. 7(b), the average resultant force progressively escalated from around 62 N to over 98 N (+58 %) across the SiC-reinforced region during conventional milling, symptomatic of the abrasive wear imposed on the cutting inserts by the hard SiC_f. In contrast, laser softening of the brittle SiC_f mitigated this tool's wear progression in both LAM configurations. Nevertheless, a slight rise in forces was still evident even with semi-inverse LAM, as shown in Fig. 7(e), suggesting potential adhesion of Ti workpiece material or some minor tool wear. Meanwhile, the forces were maintained at a near-constant level across the length of the SiC zone with fully inverse LAM, as shown in Fig. 7(h). Lastly, in the final Ti-matrix section, the average forces escalated above those measured in the initial Ti section for conventional milling, pointing to appreciable tool degradation, as depicted in Fig. 7(c). Yet for LAM, the semi-inverse approach exhibited only a minor force increase, as illustrated in Fig. 7(f). In contrast, the forces were consistent for fully inverse, as shown in Fig. 7(i), indicating minimised tool wear. This methodology provides high-resolution insight into tool wear progression through segmentation and analysis of the mean cutting forces in each zone [39]. It elucidates the thermal effects of different laser heating techniques on the mechanics of machining this non-homogenous MMC.

The obtained cutting force in conventional milling is much higher compared to LAM. More specifically, the increased heat generation in the Ti-SiC reinforcement region during conventional milling can be attributed to abrasive flank wear of the cutting tool from constant rubbing on the hard SiC fibres. This abrasive wear leads to the escalation of cutting forces over time (see Fig. 8(a)). In contrast, the laser heat assistance in LAM helps prevent this abrasive flank wear, enabling the tool to maintain sharp cutting edges longer. The uniform heat distribution in semi-inverse LAM also maintains homogeneous workpiece properties, preventing localized thermal softening that could otherwise cause non-uniform cutting forces and accelerated tool wear (see Fig. 8(b)). Conversely, the concentrated heat input in fully inverse LAM promotes selective localized thermal softening of the workpiece ahead of the cutting zone, leading to a reduction in cutting forces (see Fig. 8(c)). This allows a relatively constant level of workpiece softening for more uniform cutting forces throughout machining. The differences in heat distribution and targeted softening effects between semi-inverse and fully inverse LAM demonstrate how laser assistance can be strategically

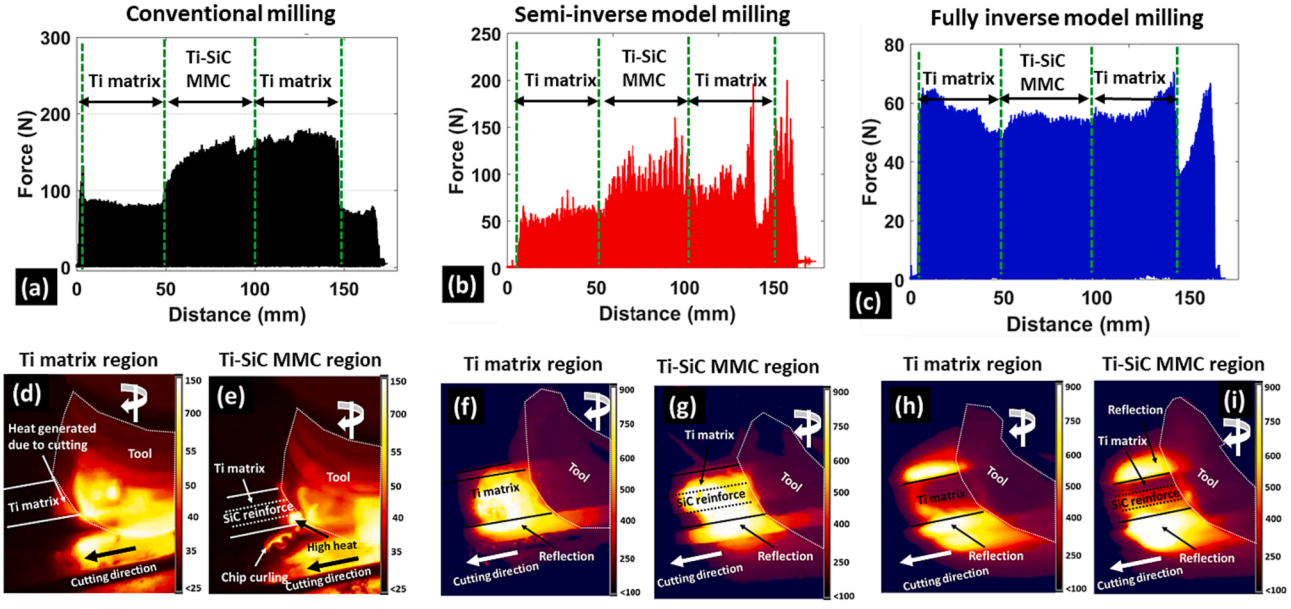

Fig. 8. Acquired cutting forces and thermal images for different LAM strategies. (a-c) The developed forces highlighting the distinct material regions for conventional milling, semi-inverse LAM, and fully inverse LAM, respectively. Thermal images depicting heat generation during the milling process at the (d,f,h) initial Ti matrix section and (e,g,i) Ti-SiC reinforced section for (d,e) conventional milling, (f,g) semi-inverse LAM, and (h,i) fully inverse LAM.

optimized to perform LAM of Ti6Al4V/SiC_f MMCs. Laser preheating enables more consistent cutting forces and improved machining performance by controlling workpiece softening and mitigating tool wear. Detailed cutting force analysis provides mechanical insights into machining this hybrid composite. Meanwhile, thermal imaging reveals how localised heat input through LAM can be fine-tuned to balance workpiece softening while counteracting the high tool wear rate when machining Ti6Al4V/SiC_f MMCs. In conventional milling, heat generation is mainly from friction between the PCD insert and MMC. Fig. 8(d) shows higher heat generation initially in the Ti matrix before contact with SiC reinforcements. In contrast, Fig. 8(e) displays greater heat generation in the Ti-SiC reinforce region, largely due to the degradation of the tool's flank edge causing rubbing instead of cutting and more heat. By integrating laser heating into LAM, the hard SiC reinforcements are softened during cutting, reducing forces, as evident from lower heat generation in the workpiece [37]. With semi-inverse LAM, thermal images exhibit high uniform heat distribution initially in the Ti matrix, which is similar in the Ti-SiC reinforce region (Fig. 8(f,g)). However, with fully inverse LAM, the heat distribution differs across material regions (Fig. 8(i)). In summary, these findings inform the selection of optimal milling conditions and LAM strategies to enhance productivity when machining this highly heterogeneous composite.

To understand the variation in cutting forces between conventional and LAM milling, the acquired raw force signals were further processed (Fig. 9). High-frequency noise was removed from the signals using a low-pass filter to identify key force trends. The filtered signals were processed to determine the average resultant cutting forces, which were compared across all milling conditions (Fig. 9). The average resultant force is reduced by 35 % in the initial Ti matrix region for fully inverse LAM compared to conventional milling. In contrast, semi-inverse LAM exhibits a 62 % lower force than other conditions in the first Ti matrix due to the high heat input from laser scanning. The average resultant force further decreases to 62 % in the Ti-SiC reinforcement region, finally reaching a 65 % reduction in the final Ti matrix region compared to conventional and fully inverse LAM. Overall, this force analysis quantitatively demonstrates that LAM, especially semi-inverse, significantly reduces cutting forces compared to conventional machining across all regions of this hybrid composite workpiece. The reduction in forces can be attributed to laser softening effects as well as reduced abrasive tool wear from rubbing on SiC particles.

4.2. Mitigating tool wear in LAM of Ti6Al4V/SiC_f MMCs

4.2.1. Influence of LAM in flank wear

Machining the hybrid Ti6Al4V/SiC_f MMC presents unique challenges owing to the mismatch between the ductile Ti- matrix and the hard, brittle SiC_f reinforcements. Flank wear initiation and evolution differ for conventional milling and LAM approaches on this specific material. Conventional milling induces rapid cutting tool wear progression dominated by micro-chipping and edge degradation mechanisms, as shown in Fig. 10(a-p) [40–42]. At the microscopic scale, the cutting edge experiences repetitive crack-forming impacts and localised brittle fracture as it sequentially encounters each SiC_f in the reinforcement region. At the macroscale, alternating engagement between the contrasting Ti-matrix and SiC_f generates cyclical stress variations that propagate edge micro-fractures over time, degrading structural integrity, as shown in Fig. 10(a-q,r,s). While machining, the tool flank face experienced a characteristic pitting and bulging due to the intergranular fracture in the cutting insert under cyclical stress variations while cutting the fibres, as shown in Fig. 10(a-s). Moreover, severe plastic deformation of the material due to progressive tool wear makes the Ti-matric stick to the edge of the cutting insert, as shown in Fig. 10(a-q).

Similarly, semi-inverse LAM reduces wear progression through uniform laser heating to soften the metal matrix compared to conventional milling, as shown in Fig. 10(b-p). The Ti-matrix absorbs the laser energy, elevating its temperature and decreasing strength before cutting occurs. Extreme softening of the Ti-matrix creates more uniform mechanical properties less similar to SiC_f, which increase cutting forces during the machining of the reinforced region, as discussed earlier. The excess softening of the Ti-matrix causes the sticking of molten Ti-matrix to the flank surface, as depicted in Fig. 10(b-q). The less temperature-influenced SiC_f retain their innate brittleness and hardness, causing

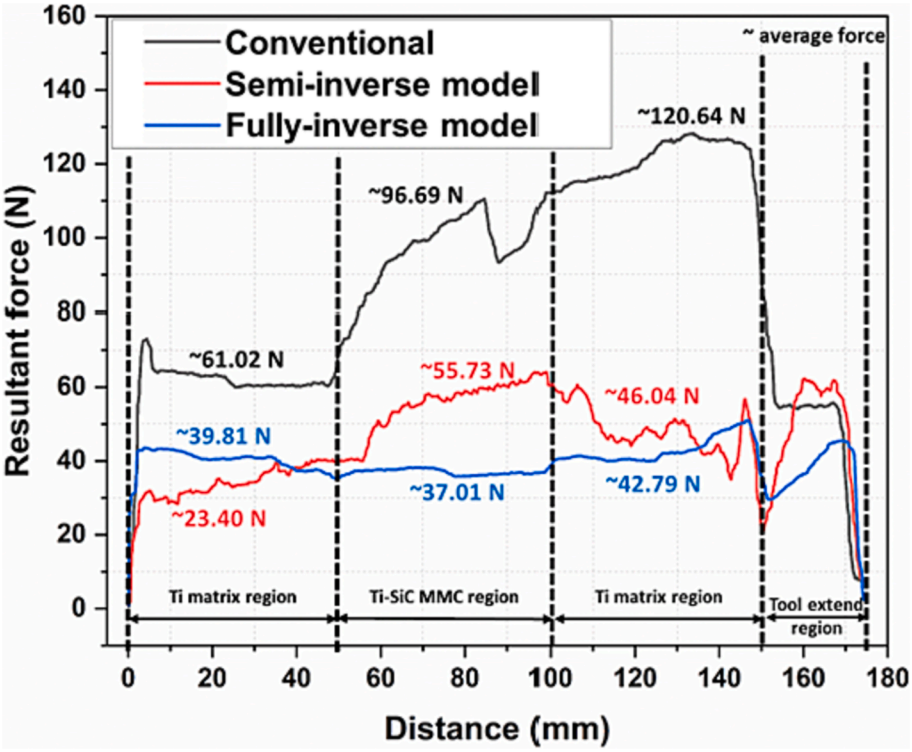

Fig. 9. Average resultant cutting force comparison showing reduced forces for LAM.

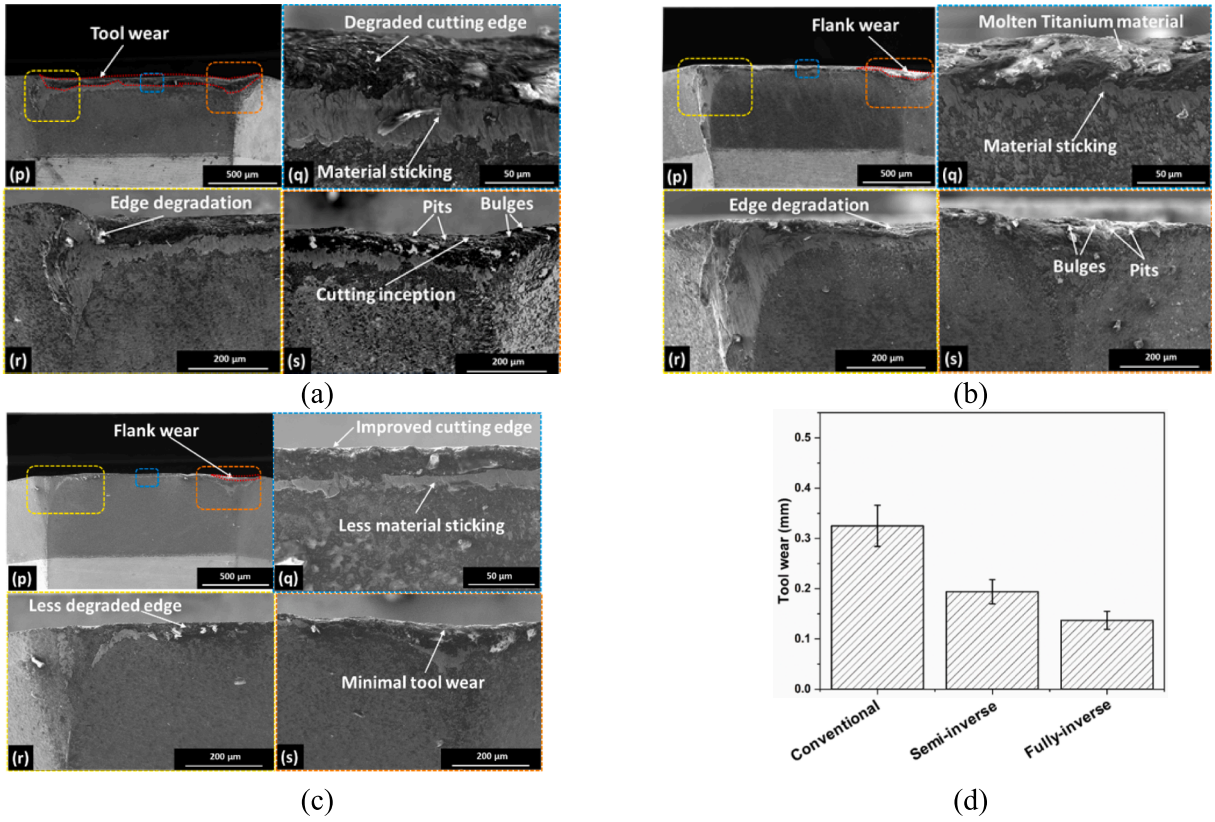

Fig. 10. Micrographs of cutting inserts (flank face) for different milling conditions: (a) conventional milling, (b) semi-inverse LAM, (c) fully inverse LAM. The subfigures specify (p) the cutting flank face, (q, r, s) the cutting edge condition in different sections - middle, left and right, respectively - and (d) the average tool flank wear for the three milling conditions.

persistent flank wear despite less than conventional milling, as shown in Fig. 10(b-r,s). Flank wear in semi-inverse indicates the need for deliberate localised reinforcement heating in fully inverse LAM to improve continuity further and mitigate variations in mechanical properties between the Ti-matrix and SiC reinforcements. Hence, fully inverse LAM uniquely minimises flank wear by incorporating distinct phase properties into its optimised localised laser heating simulations. A key benefit of controlled localised softening is mitigated thermal adhesion between the matrix and cutting tool. This promotes matrix ductility while preventing edge degradation of the cutting edge, as shown in Fig. 10(c-p). In addition, localised heating minimises the potential bonding of the matrix to the tool surface, as depicted in Fig. 10(c-q,r). Heating the SiC reinforcements with elevated temperature reduces brittle cracking and inhibits fibre fracture on the machined surface. Hence, machining the reinforced region concurrently minimises the tool flank wear. In addition, as discussed in the earlier sections, the chip-tool contact is also decreased, which minimises the Ti-matrix sticking with the cutting insert. In summary, machining MMCs poses unique difficulties due to the mismatch between the ductile, Ti-matrix and hard, brittle SiC_f reinforcements. Fig. 10(d) depicts the average tool flank wear for different milling conditions. Conventional milling suffers from rapid flank wear of ~ 0.35 mm due to edge degradation. In contrast, LAM techniques offer a promising solution for tool wear. The observed tool flank wear in the semi-inverse LAM is ~ 0.19 mm, almost a 50 % improvement compared to conventional milling. Fully inverse LAM uniquely minimises flank wear of ~ 0.14 mm by incorporating distinct material properties into optimised simulations. In essence, fully inverse LAM provides substantial tool life enhancement in machining Ti6Al4V/SiC_f MMC by optimally alleviating edge degradation, pits and bulges through deliberate laser-material coupling informed by multi-physics modelling. Further, the tool wear can be justify by the reduced cutting forces in LAM minimise stress at the tool-workpiece interface, which minimises abrasive and adhesive wear on the cutting tool [43]. Softening the matrix improves load transfer between matrix and fibres by reducing stress concentrations at fibre–matrix interfaces [44,45]. As a result, the cutting tool is less likely to become blunted through abrasive wear due to fibre fractures [43]. Further to tool flank wear it is necessary to study the rake wear for better understanding the chip morphology.

4.2.2. *Influence of LAM in rake face wear*

The rake wear mechanism differs markedly between conventional milling techniques, and LAM approaches when machining MMCs. As shown in Fig. 11(a,b), conventional milling produces rapid rake wear caused by cyclical impacts against hard SiC_f that oxidise and degrade the tool binder in the rake face. Thermal variations caused by alternating tool engagement between ductile matrix and brittle reinforcement drive the binder used in PCD tool protrusion and accelerate tool wear.

According to Fig. 11(c,d), semi-inverse LAM reduces rake wear progression by uniformly preheating the matrix before cutting, which results in fewer micro-craters. As shown in Fig. 13 (f,i), some of the fragmented SiC particles adhere to the chip backside, which inhibits the reaction between the binder and SiC particles, resulting in less chipping. As shown in Fig. 11(d), some molten Ti-matrix adheres to the surface of the rake when excessive heating occurs. As shown in Fig. 11(e,f), the thermal profile is tailored to avoid binder oxidation and protrusion, preventing chipping and micro cratering. By optimising laser-material coupling informed by modelling, fully inverse LAM increases tool rake life by balancing fibre fracture and binder oxidation mechanisms. It is possible to achieve deliberate rake face protection using the physics-based approach, which is impossible with conventional techniques.

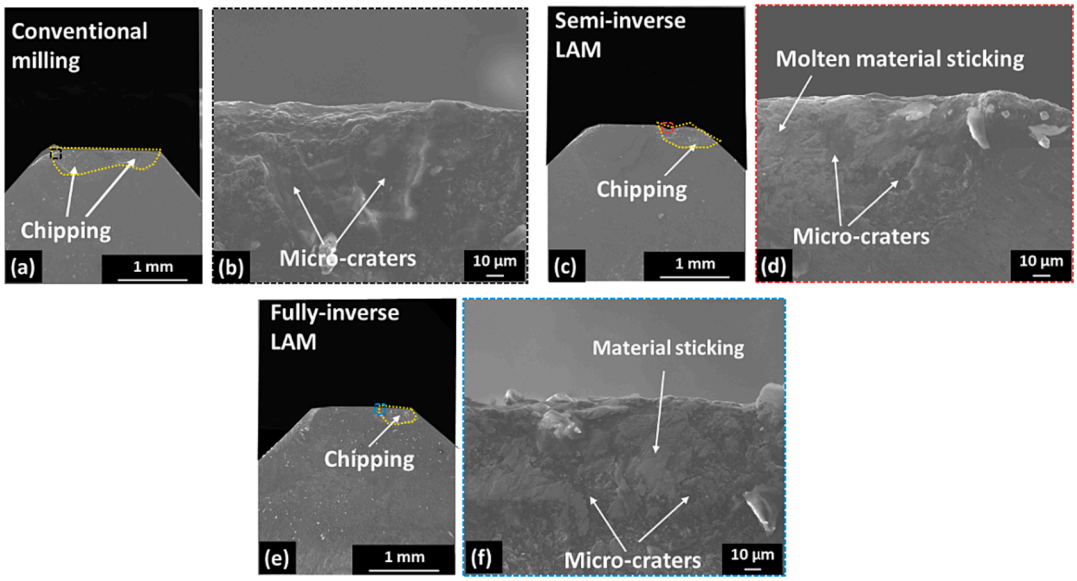

Fig. 11. Micrographs of cutting inserts (rake face) for different milling conditions: (a,b) conventional milling, (c,d) semi-inverse LAM, (e,f) fully inverse LAM.

4.3. Investigating importance of chip curling and void formation in segmented chip for conventional milling and LAM

Investigating chip morphology provides critical insights into the machining mechanics and shear phenomena occurring during cutting. Analysing factors such as chip curling, segmentation, and void formation reveals key differences in the cutting behaviour between conventional milling and LAM of this composite. Fig. 12 (a) illustrates the schematic of the cutting mechanism between the tool and workpiece during conventional milling. An enlarged view in Fig. 12(b) shows how an individual cutting insert shears the workpiece and highlights chip formation when machining the Ti6Al4V/SiC_f MMC. For the chosen parameters, the cutter takes a 0.05 mm a_e and 0.2 mm a_p across the workpiece's 10 mm wide reinforced region. The rotating tool generates segmented chips through intermittent engagement, as depicted in Fig. 12(c). Cross-sectional images reveal distinct chip regions—the a_e

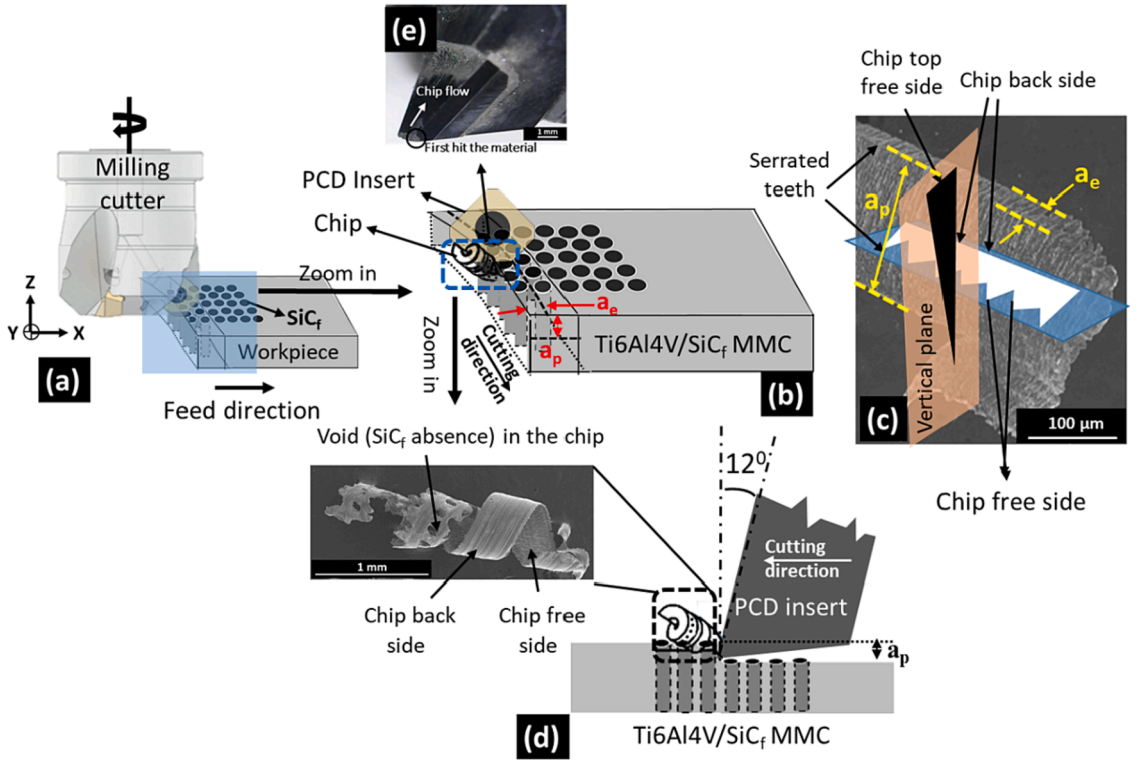

Fig. 12. Schematically illustrates chip formation and flow during conventional milling of a Ti6Al4V/SiC_f MMC: (a) shows the overall tool-workpiece engagement, (b) presents an enlarged view of a single cutting insert milling the composite, highlighting the underlying chip generation mechanisms, (c) depicts the key features of a cross-sectioned chip obtained from milling the MMC, including the serrated top free-side and smoother back side, (d) shows modelled chip formation in the SiC reinforced region, where the positive rake angle induces upcurling of the discontinuous chips and (e) portrays the rake face of the cutting tool containing a chip breaker element.

dimension matches the chip serrations and top-free surface. At the same time, a_p corresponds to the serrated chip-free surface, as shown in Fig. 12 (c). This visualisation enables us to understand better void formation within chips produced in the reinforcement zone. Fig. 12(d) presents a detailed schematic of chip formation within the SiC_f reinforced region. As the cutting tool shears the composite material, the interactions at the tool-workpiece interface depend on the localised material composition. Within the Ti-matrix, continuous chips are formed by plastic deformation of the ductile metal. However, upon encountering a hard, brittle SiC_f, a fracture occurs, resulting in discontinuous chip formation. The reinforcing fibres resist plastic deformation and cutting, instead fracturing from the compressive and shear stresses the cutting tool exerts. This intermittent fracture of SiC_f leads to chip segmentation, as shown in Fig. 12(d). The voids observed in the chips from this region arise from the absence of fibre where a SiC_f has fractured and disengaged from the surrounding Ti matrix. Based on this observation, it has been concluded that the size of the fibre, spacing between the fibre, and properties of the reinforcing fibres in the composite dictate the formation of chip segmentation. Moreover, the high thermal gradients and rapid heating/cooling transients inherent to the LAM process can alter chip morphology and segmentation [46]. In conventional milling, it is crucial to prevent chip adhesion to the cutting insert, which increases cutting forces, wear, and surface defects [31]. With LAM, the chip adhesion can be better controlled during milling because the chip geometry has been altered due to thermal heating [47]. As shown in Fig. 12(e), the discontinuous chips generated in the reinforced region flow along the cutting tool's rake face at an angle of 12° before undergoing additional fragmentation. The positive rake angle helps curl the chips, aiding chip evacuation across the rake face [48,49]. However, the segmented nature of the chips produced when cutting the SiC_f results in a jagged chip flow pattern along the tool. The discontinuous chips are more prone to cracking and breaking than continuous chips from monolithic metals. A chip breaker feature is often incorporated above the cutting edge to control chip segmentation. The protruding chip breaker induces additional bending and fragmentation of the chips through mechanical loading as they flow across the rake face. This helps break the chips into smaller pieces that can be efficiently evacuated from the cutting zone [50,51]. The chip breaker is particularly useful when milling the SiC-reinforced composite, where the disparate properties and chip morphologies between the two materials otherwise lead to long chip formation. In summary, the complex tool-workpiece interactions while machining the non-homogenous composite necessitate chip breaker elements and tailored rake angles to facilitate chip flow and achieve desirable segmentation for efficient chip evacuation. Hence, this information provides insight into chip segmentation mechanics, void formation, and chip flow resulting from the intricate cutting tool-workpiece interactions inherent to milling this non-homogenous composite material.

In conventional milling of Ti6Al4V/SiC_f MMCs, the chip morphology and segmentation formed in the chips are influenced by critical cutting parameters, including cutting speed, feed rate, depth of cut, and tool geometry. The chosen PCD tool, with a 45° edge angle, generates discontinuous and serrated chip shapes characteristic of segmented chip formation, as shown in Fig. 13(b). However, the brittle fracture of the reinforcing SiC_f and the resulting chip segmentation also contribute to accelerated abrasive wear of the PCD tool. These brittle fractures often result in voids with high circularity in the chips, appearing as rounded holes, as depicted in Fig. 13(c). A key aspect governing chip formation is the twist angle, defined as the angle at which the chip curls or spirals during the cutting process [49]. Conventional milling typically produces higher twist angles based on the mechanics of the oblique cutting process, as depicted in Fig. 13(a). Higher twist angles extensively fragment the chips and increase the number of tool-chip contacts, potentially accelerating tool wear. However, it further increases chip adhesion and

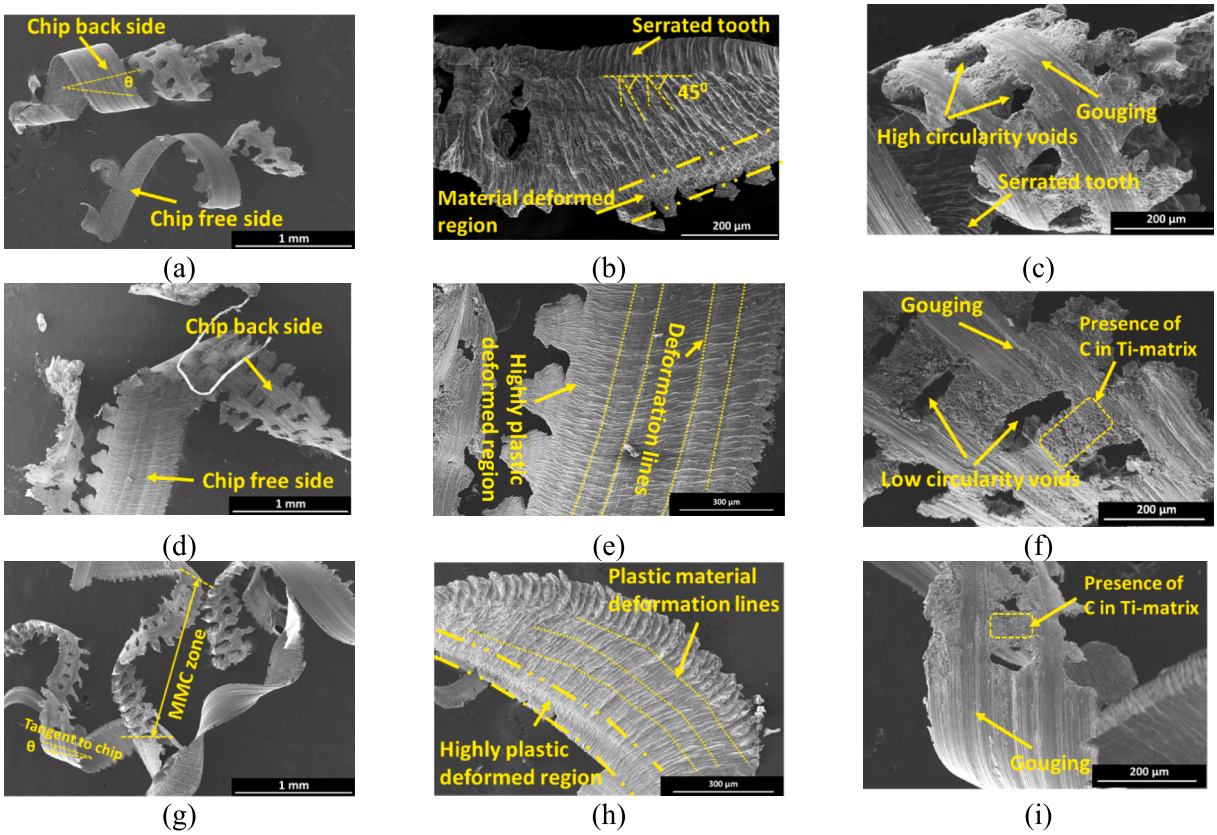

Fig. 13. Chip morphology of milled Ti6Al4V/ SiCf MMC: (a-c) Conventional milling, (d-f) Semi-inverse LAM, and (g-i) Fully inverse LAM, (a,d,g) details the variation in twist angle (θ), (b,e,h) and (c,f,i) highlights the chip free side and back side, respectively.

cyclic loading from the serrated chip-tool interactions, increases cutting forces and hinders smooth chip flow in the rake face. As mentioned, LAM integrates laser heating to thermally soften the Ti6Al4V/SiC_f MMC workpiece before tool engagement. In semi-inverse LAM, the laser uniformly heat induces thermal softening of the Ti-matrix approaching the cutter, altering chip formation compared to conventional milling. The softened Ti-matrix promotes chip flow at lower shear stresses, which lowers the twist angles as the chips curl, resulting in less intense chip segmentation. This segmentation reduction is associated with insufficient chip adhesion to the cutting tool. Semi-inverse LAM chips exhibit more continuous profiles and ductile shearing from the heated Ti-matrix, forming shear banding and deformation lines, as depicted in Fig. 13(e). Since the SiC_f are not fracturing, the voids form in the generated chip exhibit irregular shapes, i.e., lower circularity dictated by the soft Ti-matrix chip flow around the hard SiC, as shown in Fig. 13 (f,i). In fully inverse LAM, optimised laser trajectories account for the distinct thermal properties of the Ti-matrix and SiC reinforcement phases. The customised laser modulation carefully controls thermal gradients ahead of the cutter. This allows further reduction of the twist angles, as depicted in Fig. 13(g), compared to conventional milling, indicating an improved surface finish and reduction in cutting forces. The highly localised matrix softening facilitates continuous chips with minimal segmentation that can slide smoothly for efficient evacuation. Localised heating on Ti-matrix hinders plastic flow, causing a decrease in discrete shear bands and deformation lines compared to semi-inverse LAM, as depicted in Fig. 13(h). With the fully inverse LAM of this non-homogeneous MMC, a detailed study of the resulting chip morphologies provides critical insight into thermal damage effects and the shape of void formation in the reinforcement region.

4.4. *Evidence of LAM has an influence in improving surface morphology and reducing roughness*

Surface morphology and roughness measurements provide critical insights into the machining mechanics and resulting quality of the composite workpiece. Comparing the macroscopic surface characteristics under different milling conditions elucidates the effects of LAM on the cutting behaviour of this non-homogeneous material. A macroscopic examination of the machined surfaces, as shown in Fig. 14, reveals differences in surface quality between the three milling conditions, revealing the underlying cutting mechanisms of non-homogenous materials. The surface morphology in the middle of the reinforced region is shown for all cutting conditions. As depicted in Fig. 14(a), the conventional milling process results show an extensive SiC_f fracture and fibre drag on the surface. Alternate interaction of cutting inserts with the SiC_f generates local vibrations within the fibres, causes fibre debonding with the Ti-matrix, fibre fractures on the top surface, and also leads to propagation of microcracks within the SiC cover surrounding the ductile tungsten core, as depicted in Fig. 14(d). Due to the limited heat generated during conventional milling, the carbon coating around the SiC_f remains undamaged. It is non-reactive with the titanium matrix, as shown in Fig. 14(d). Additionally, the progressive wear of the tool contributes to increased cutting forces, leading to intense fibre fracture over time. Due to the absence of external heat generation, conventional milling produces elevated cutting temperatures primarily due to friction between the cutting tool and workpiece and plastic deformation of Ti-matrix. As a result of the continuous progression of tool wear, cutting forces escalate over time, which increases the risk of fibre fracture, as shown in Fig. 14(a,d). Moreover, the non-homogeneous material combination causes inconsistent tool-workpiece engagement between the SiC reinforcement regions and the softer Ti-matrix. It results in localised tearing and smearing of the ductile Ti surrounding the fractured SiC_f. Transitioning from conventional milling, semi-inverse LAM reveals intriguing behaviours. This technique involves uniform laser heating across the Ti-SiC reinforcement regions to induce more consistent thermal softening. This heat distribution aims to achieve more homogeneity in the material's response to thermal stresses. However, it is essential to note that while this technique offers advantages in achieving thermal uniformity, prolonged exposure to elevated temperatures in the Ti-matrix can potentially give rise to some undesirable effects. One such effect is the risk of thermal damage, which can manifest in oxidation and localised melting. This is particularly relevant due to the inherent reactivity of materials, such as Ti, SiC_f and carbon coating around the fibres, with oxygen at elevated temperatures, as shown in Fig. 14(e,f). Oxidation can alter the chemical composition of the surface, leading to a loss of material integrity and potentially compromising mechanical

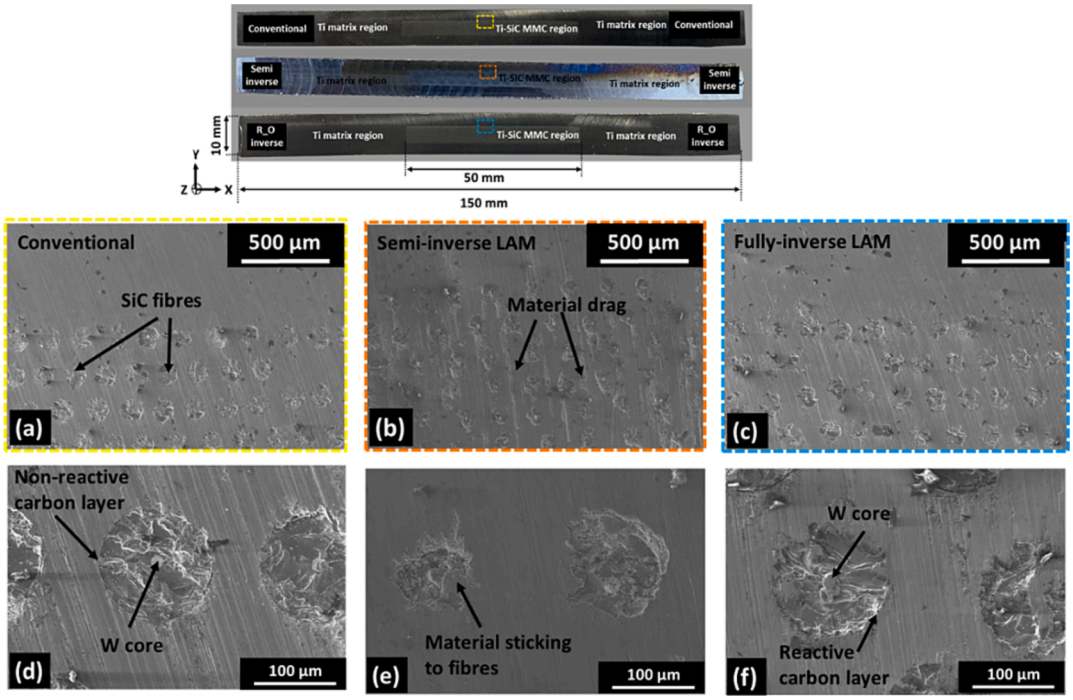

Fig. 14. The surface morphology of the different milling conditions (a,d) conventional milling, (b,e) semi-inverse LAM, and (c,f) fully inverse LAM.

properties, as discussed in later sections. Furthermore, as the duration of elevated temperature exposure increases, there is a corresponding elevation in the degree of adhesion between the thermally softened Ti material, which sticks in the fibre region, as shown in Fig. 14(e). The intensified adhesion can manifest as significant feed marks due to Ti plastic deformed material drag on the machined surface, as shown in Fig. 14(b). The interplay between the uniform thermal softening induced by semi-inverse LAM and the potential challenges associated with thermal damage and increased tool adhesion adds a layer of complexity to the machining process.

As a result, meticulous control of laser parameters and exposure durations becomes pivotal to striking a balance between achieving desirable thermal effects and mitigating potential drawbacks based on surface integrity. In contrast, fully inverse LAM employs highly localised laser heating confined precisely to the cutting zone. The model induces a sharply localised temperature, focusing thermal softening exclusively on the titanium matrix and SiC-reinforced regions before tool engagement. By concentrating heat input on the Ti-matrix phase, fully inverse LAM minimises conduction heating of the adjacent SiC_f in the Ti-SiC reinforce region. It reduces Ti-matrix's reactivity with carbon coating compared to semi-inverse LAM. The confined matrix softening in fully inverse LAM achieves two pivotal objectives. Primarily, it enables precise thermal alteration of the Ti-matrix to reduce cutting forces. Critically, it avoids bulk heating that could induce thermal degradation of the inherently brittle SiC reinforcements. This selective laser application prevents excessive heating of the Ti-matrix, which is susceptible to microstructural changes and embrittlement of Ti-matrix at high temperatures. Therefore, the strategic localisation of the thermal assistance is imperative to simultaneously improve machinability through matrix softening while preserving the structural integrity of the SiC reinforcement. Consequently, SiC_f fragmentation and ploughing forces, which roughen surfaces in conventional milling, are markedly reduced, as depicted in Fig. 14(f). The selective laser application curtails deleterious adhesion while enabling sufficient matrix softening to improve surface finish, as shown in Fig. 14. Laser integration in fully inverse LAM balances targeted thermal benefits while avoiding drawbacks of excessive heat generation observed in semi-inverse LAM. The targeted thermal effects in fully inverse LAM conclude in markedly smoother surfaces with reduced feed marks, enhancing surface finishing as shown in Fig. 14(c,f). The precision control of localised laser assistance also preserves the composite's structural integrity, which is discussed in later sections.

The visual surface morphology observations described above could also support the quantitative surface roughness measurements. To characterise the surface roughness, observations were conducted at the centre of the samples, 50 mm along the length, to evaluate the effect of laser heating on the surface finish. As shown in Fig. 15(a,c,e), the conventionally milled sample surface exhibits intense SiC_f fracture evident from the fibre drag marks. However, with semi-inverse LAM, the plasticised Ti matrix is dragged over the fibres during milling. In contrast, fully inverse LAM produced a smooth surface topography devoid of SiC_f or Ti matrix drag marks along the feed direction, as depicted in Fig. 15(e). The 3D surface profiles in Fig. 15(b,d,f) provide the mean surface height used to quantify surface roughness. The conventional and semi-inverse LAM samples have comparable and higher mean surface heights owing to intense SiC_f fracture and Ti matrix drag effects, respectively. However, the mean size for fully inverse LAM is approximately 25 % lower than conventional milling, as shown in Fig. 15(g), indicating an improved surface finish. The average surface

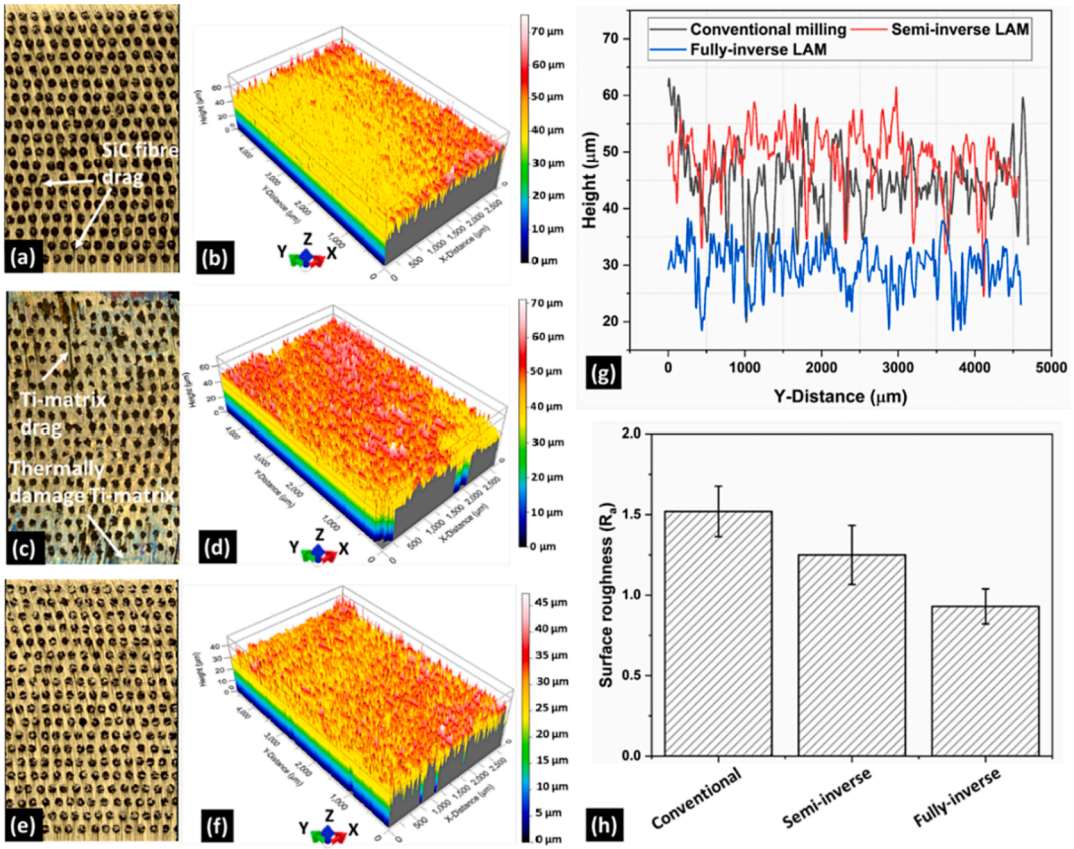

Fig. 15. Surface morphology and roughness for conventional and LAM of Ti6Al4V/SiC_f composite are examined: (a) and (b) show intense SiC_f fracture and higher mean surface height from conventional milling, (c) and (d) present reduced fibre damage but Ti matrix drag causing intermediate roughness with semi-inverse LAM, (e) and (f) demonstrate fully inverse LAM produces the smoothest surface with minimal drag marks or height variations, (g) directly compares the lower mean height for fully inverse LAM versus conventional milling and (h) depicts the average surface roughness (R_a) values to quantify the substantial roughness decrease achieved with fully inverse LAM.

roughness (R_a) was measured for further insight, as presented in Fig. 15 (h). Conventional milling exhibited the highest R_a of 1.52 μm, consistent with the substantial fibre fracture and matrix ploughing effects. This increased surface roughness stems from the aggressive tool-workpiece interactions that induce surface irregularities during conventional machining without targeted heating. In comparison, semi-inverse LAM resulted in a more moderate R_a of 1.25 μm, arising from the trade-off between thermal softening benefits and potential overheating drawbacks. The minor material drags and thermal damage from sustained heating contribute to this surface roughness, though it remains a better surface finish than conventional milling. Fully inverse LAM demonstrated the most promising enhancement in surface quality, with the lowest R_a of 0.93 μm. This 62 % reduction compared to conventional milling highlights the effectiveness of fully inverse LAM. Optimised localised thermal softening is critical, enabling a smooth finish by reducing cutting forces and wear and mitigating fibre fracture and matrix adhesion issues in the composite region. Thus, the quantitative roughness data, supported by visual characterisation, proves that fully inverse LAM effectively limits surface defects by controlling tool-workpiece interactions through selective laser heating. This balanced approach improves finish quality substantially. The thorough surface analysis provides valuable mechanistic insights and demonstrates the merits of strategic laser integration for advancing the surface quality of the milling MMCs.

4.5. Influence of LAM in surface integrity variation in machining highly heterogenous MMCs

Machining MMCs like Ti6Al4V/SiC_f using conventional milling methods results in severe degradation of surface integrity and extensive microstructural damage. The alternating engagement between the ductile Ti-matrix and SiC_f reinforcements experiences concentrated stresses at the points of contact with the cutting tool edges [15]. The stresses concentrate on the hard reinforcement-soft matrix interfaces and the precise tool-fibre interaction loci. This leads to the fracture of the brittle SiC_f and extensive surface defects in conventional milling. Surface defects like fibre pull-out, uncut protruding fibres, fibre cracks and surface cracking are observed due to the mismatch in properties and high stresses, as shown in Fig. 16(a) [15]. In addition, severe plastic deformation is observed on the machined surface due to progressive tool wear, which occurs from direct abrasive contact with SiC_f during milling. Therefore, strategies to improve Ti6Al4V/SiC_f MMC machinability should aim to minimise and redistribute concentrated subsurface stresses to avoid reinforcement fracturing and sub-surface defects that degrade the final machined surface quality. In this regard, semi-inverse LAM reduces some surface defects compared to conventional milling by uniformly pre-heating the entire matrix to soften it before cutting. However, the reinforcements still produce direct surface damage, like partial fibre pull-outs and fibre cracks, as shown in Fig. 16(b). Microstructurally, fewer fibre fractures on the machine surface are present but substantially eliminate the surface cracks.

More significantly, the widespread matrix heating enables increased atomic diffusion, promoting a reaction between the Ti-matrix and carbon coatings on the SiC_f. This results in excessive growth of Ti_2C dendrites in the matrix around fibres compared to conventional methods, as depicted in Fig. 16(b). Fully inverse LAM provides the optimal strategy by localising laser heating only to matrix zones bordering the reinforcements just before cutting. This prevents direct tool-fibre contact and associated surface defects. Deformation is confined to a small thermally-affected matrix region, minimising damage, as depicted in Fig. 16(c). Microstructurally, fibre fractures and interface cracks are also significantly reduced through tailored stress relief. Localised bulk Ti-matrix heating restricts atomic mobility, which better controls the Ti_2C interfacial reaction, as shown in Fig. 16(c), compared to extensive dendrite formation in semi-inverse LAM. Further, the sub-surface defects for each milling condition are analysed in detail in the next section.

4.6. Proof that LAM has influence in sub-surface variation revelled using EBSD analysis

Machining MMCs conventionally leads to extensive microcracking within the plastically deformed matrix grains due to highly concentrated stresses during milling. The repetitive, alternating engagement between the soft matrix and exceedingly hard ceramic reinforcements generates severe localised shear deformation bands in the metallic phase. These deformation zones create stress concentrations at grain boundaries and triple junctions, from which microcracks initiate. Propagation occurs rapidly along preferential slip planes aligned to the cutting direction as the localised stresses exceed the fracture strength of the matrix. Extensive transgranular microcracking provides connected fracture paths that allow cracks to link up and enable intergranular failure, as depicted in Fig. 17(a). LAM approaches significantly suppress microcracking in the Ti-matrix by controlling deformation instabilities through deliberate laser heating strategies. Semi-inverse LAM applies uniform laser heating across the entire MMC before cutting. This pre-heating enables a more homogeneous plastic flow of the Ti-matrix during machining by softening the material. The uniform thermal softening reduces stress concentrations, and limits localised brittle fracture zones by distributing applied stresses evenly throughout the ductile matrix. Additionally, the extensive bulk heating of the Ti-matrix in semi-inverse LAM promotes atomic diffusion, enabling increased reaction between the titanium and carbon coatings on the SiC_f reinforcements. The high mobility of Ti atoms due to thermal activation facilitates interaction with the C coatings. This results in the excessive formation of titanium carbide (Ti_2C) intermetallic compound dendrites growing from the fibre–matrix interface into the titanium matrix, as depicted in Fig. 17(c). The extensive pre-heating enables sufficient atomic diffusion distances for these brittle Ti_2C dendrites' accelerated growth compared to conventional methods or fully inverse LAM. Therefore, while semi-inverse LAM suppresses microcracking through uniform matrix flow, uncontrolled bulk heating also undesirably enhances Ti_2C intermetallic formation. This highlights the need for deliberate tailoring of thermal effects by location to optimise the balance between matrix softening, microcrack resistance, and interfacial reaction control. Fully inverse LAM provides

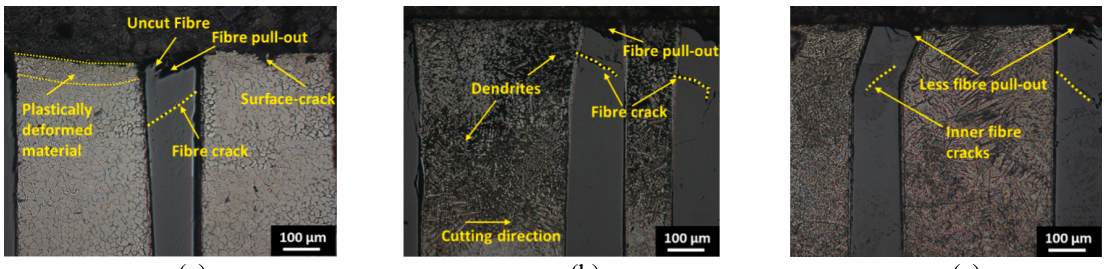

Fig. 16. Microscopy images of sub-surface defect for different milling conditions: a) Conventional, (b) semi-inverse LAM, and (c) fully inverse LAM.

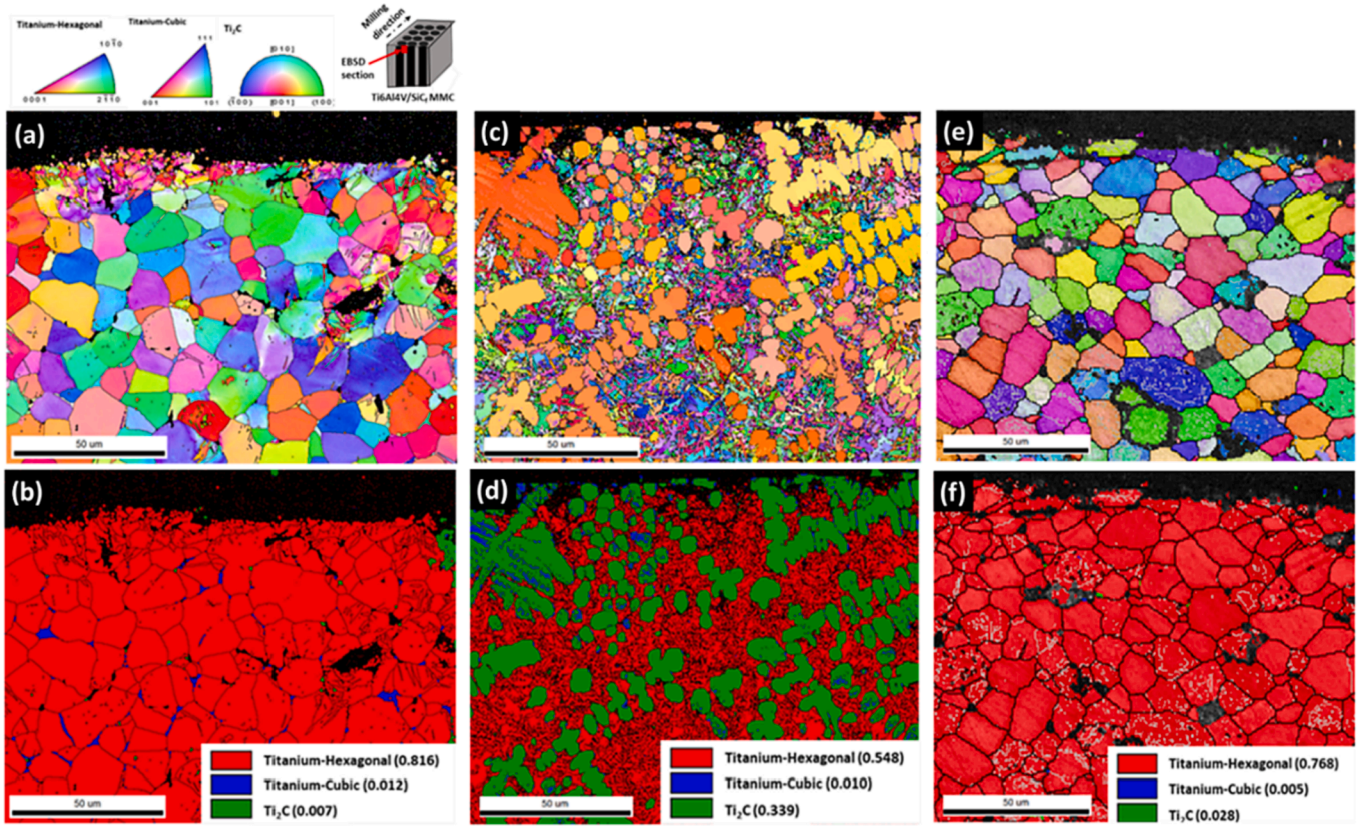

Fig. 17. EBSD analysis of the Ti-matrix cross-section under (a,b) conventional milling, (c,d) semi-inverse LAM, and (e,f) fully inverse LAM conditions. (a,c,e) The Euler angle maps reveal the grains and microcracks under each condition. (b,d,f) are phase identification maps showing the phases after machining.

the optimal approach by localising laser heating between the Ti matrix zones and the reinforcement region just before cutting. This highly selective localised heating minimises concentrated stresses in the Ti-matrix while direct tool-reinforcement interactions. As a result, fully inverse LAM with strategically localised heating at fibre–matrix interfaces provides superior microcrack resistance compared to conventional milling, as shown in Fig. 17(e). The confined heating in fully inverse LAM limits atomic diffusion distances, restricting the excessive growth of Ti_2C intermetallics. Thermal activation is constrained to the small volume surrounding the fibres, preventing bulk matrix softening and uncontrolled reactions. Therefore, fully inverse LAM uniquely optimises the trade-off between targeted matrix softening to reduce microcracks while deliberately controlling interfacial reactions by selective spatial tailoring of heat application. This balancing of competing objectives for enhanced machinability is unattainable through conventional bulk processing methods. As a result, both semi-inverse and fully inverse LAM substantially reduce matrix grain microcracking density compared to conventional milling based on the microstrual observations. Beyond microcracking effects, the fraction of metastable β-Ti phase in Ti6Al4V matrix composites also varies significantly between conventional milling and LAM, as depicted in Fig. 17(b,d,f). Conventional milling induces extreme plastic deformation in the matrix from the high mechanical loads exerted during cutting at the tool-material interface. This concentrated severe plastic deformation results in dynamic recrystallisation of the Ti-matrix grains at the surface. Forming new strain-free grains reduces the non-equilibrium β-Ti phase compared to the bulk alloy. The localised frictional heating generated at the high shear stress bands enables thermal driving forces for β-Ti decomposition. The combined effects of deformation-induced recrystallisation and thermal decomposition at elevated machining temperatures cause a marked decrease in the metastable β-Ti phase percentage compared to the unmilled MMC. In contrast to conventional methods, LAM approaches better restrict the intensity of matrix plastic deformation by pre-softening the material through laser heating. This reduces strain accumulation and limits the driving forces for recrystallisation and associated metastable β-Ti destabilisation. Additionally, the rapid heating and cooling thermal cycles inherent to LAM induce diffusion less transformations that alter phase fractions. The high heating and cooling rates can promote the formation of non-equilibrium martensitic α -Ti' instead of the equilibrium α-Ti. When the laser heats the MMC beyond its beta-transus temperature, the decomposition rate of β-Ti at high temperatures exceeds its growth rate according to kinetics. This transiently shifts the thermodynamic equilibrium to form α-Ti over β-Ti preferentially. Subsequent rapid cooling into the bulk lattice generates thermal gradients that facilitate α-Ti' martensite nucleation. The martensitic transformation enables retention of the laser-induced shift towards the α phase field, impeding the regrowth of β-Ti. Furthermore, the semi-inverse LAM approach applies uniform laser heating across the entire bulk matrix region. This pre-heating of the matrix enables annealing effects, which annihilates some dislocations through recrystallisation processes. The reduction in dislocation density moderates stabilising the metastable β-Ti phase by minimising available heterogeneous nucleation sites. However, semi-inverse LAM involves direct contact between the cutting tool and unsoftened fibre reinforcements during machining. This localised interaction induces deformation in the matrix surrounding the reinforcements, generating additional dislocations. These deformation zones retain and even facilitate further formation of β-Ti particles, as depicted in Fig. 17(d). Therefore, while the uniform matrix heating in semi-inverse LAM reduces β-Ti content by recrystallising other areas, the uncontrolled tool-reinforcement engagement still concentrates strain and enables localised retention of β-Ti particles around reinforcements. This highlights the deficiencies of semi-inverse techniques in fully controlling microstructural evolution. Optimised spatial tailoring of thermal softening paired with minimised

deformation is very much required. In this regard, fully inverse LAM minimises both plastic deformation and β-Ti stabilisation effects by optimising selective laser heating of the matrix-reinforcement interface just before cutting. The highly localised heating softens the matrix without affecting the bulk alloy, preventing concentrated deformation from occurring during machining. Simultaneously, the tailored thermal profile applied at the precise region allows metastable shifting of phase fractions and induction of non-equilibrium microstructures. As depicted in Fig. 17(f), a significant retention of α-Ti compared to the equilibrium β-Ti phase due to the formation of martensitic α-Ti' phases as discussed earlier. Such strategic engendering of metastable localised phases is only achievable through the physics-based modelling and control of laser-material interactions unique to LAM processing.

5. Conclusions

Due to their high specific strength and stiffness, MMCs reinforced with continuous ceramic fibres like SiC have emerged as advanced structural materials for aerospace applications. However, machining long fibre-reinforced MMCs such as Ti6Al4V/SiC_f poses significant challenges arising from the mismatch between the ductile titanium alloy matrix and the brittle SiC_f reinforcements. While the orderly composite structure with alternating ductile and brittle phases enables exceptional mechanical properties, the interactions between the two contrasting material phases during machining are poorly understood. This study performed milling processes with conventional and LAM experiments on Ti6Al4V/SiC_f MMCs to provide insights into the cutting mechanisms. Milling was carried out using PCD tool material under different conditions (i.e. conventional, semi-inverse LAM and fully inverse LAM) to study the variations in cutting forces, chip morphology, and surface finish. In addition, SEM and EBSD analysis was performed on the cross-section of the machined samples to study the effects of plastic deformation and laser heating on grain refinement and deformation. The tool wear analysis of long fibre-reinforced MMCs and the effect of laser preheating on machining results are explained based on the experimental investigations. The significant findings of this research can be summarised as follows:

- The fully inverse model optimises separate temperature fields for the Ti-matrix and SiC_f regions, avoiding issues with traditional LAM methods that apply uniform heating. By accounting for the distinct thermal properties of each phase, fully inverse LAM provides unprecedented control over localised matrix softening while preventing thermal damage to fibres.
- Semi-inverse LAM with uniform heating along the MMC was able to achieve a 43 % reduction in cutting force, whereas fully inverse LAM, i.e. localized heating, substantially reduced cutting forces compared to conventional milling, with up to a 62 % decrease in the reinforced region. This is attributed to localized matrix softening. The lower forces mitigate abrasive tool wear from tool-fiber contact.
- Conventional milling produced segmented chips with high twist angles, increasing tool-chip contact and wear. Laser assistance thermally softened the matrix, reducing the twist angles and segmentation by promoting localised plastic flow. The chip morphologies revealed the effects of laser-induced matrix heating on curling and continuity. Fully inverse LAM enabled the most continuous chip formation through optimised laser modulation and localised matrix heating.
- Conventional milling of the MMC resulted in rapid flank wear progression of ~ 0.35 mm due to cyclical impacts and edge degradation when cutting the brittle SiC_f. In contrast, semi-inverse LAM reduced average flank wear to ~ 0.19 mm, a 46 % improvement, by uniformly preheating the matrix. Fully inverse LAM enabled a 60 % reduction in moderate flank wear to ~ 0.14 mm compared to conventional milling by optimising localised laser heating through modelling. This minimised thermal adhesion and edge degradation during reinforced region cutting.
- Conventional milling of the Ti6Al4V/SiC_f metal matrix composite induced extensive microcracking, grain distortion, and destabilisation of the metastable β-Ti phase in the titanium alloy matrix due to severe plastic deformation and localised stress concentrations. LAM approaches significantly reduced microcracking density and grain distortion by thermally softening the matrix to enable more homogeneous deformation. However, uncontrolled bulk heating in semi-inverse LAM caused excessive formation of brittle Ti2C intermetallics. Fully inverse LAM with optimised localised laser heating at the matrix-reinforcement interface provided the best microcrack resistance and microstructural control. Tailored thermal profiles minimised deformation while retaining grain orientations and enabling non-equilibrium phase transformations.

CRediT authorship contribution statement

Omkar Mypati: Writing – original draft, Visualization, Validation, Methodology, Investigation, Formal analysis. **Jeriel Panzer:** Validation, Formal analysis. **Jose A. Robles-Linares:** Writing – review & editing, Investigation. **Shusong Zan:** Writing – review & editing, Formal analysis. **Zhirong Liao:** Writing – review & editing, Supervision, Methodology, Funding acquisition, Formal analysis, Conceptualization. **Dragos Axinte:** Writing – review & editing, Supervision, Funding acquisition, Formal analysis, Conceptualization.

Declaration of competing interest

The authors declare the following financial interests/personal relationships which may be considered as potential competing interests: Zhirong Liao reports financial support was provided by Innovate UK. Zhirong Liao reports financial support was provided by Smart Eureka. If there are other authors, they declare that they have no known competing financial interests or personal relationships that could have appeared to influence the work reported in this paper.

Data availability

Data will be made available on request.

Acknowledgements

The authors gratefully acknowledge the THERMACH project (Innovate UK Grant No. 74744, SMART Eureka Grant No. S0313)" for sponsoring this research. The authors gratefully acknowledge TISICS Ltd. for supplying the material and Seco Tools UK for providing the necessary cutting tools used in this research. The authors gratefully acknowledge the OpTek systems for laser integration. The authors are grateful to the Nanoscale and Microscale Research Centre (nmRC) for providing access to the SEM, EBSD facilities and for the kind support from Nigel Neate.

Appendix A. Supplementary data

Supplementary data to this article can be found online at https://doi.org/10.1016/j.matdes.2023.112552.

References

[1] Z. Liao, A. Abdelhafeez, H. Li, Y. Yang, O.G. Diaz, D. Axinte, State-of-the-art of surface integrity in machining of metal matrix composites, Int. J. Mach. Tool Manu. 143 (2019) 63–91, https://doi.org/10.1016/j.ijmachtools.2019.05.006.
[2] C. Tan, F. Weng, S. Sui, Y. Chew, G. Bi, Progress and perspectives in laser additive manufacturing of key aeroengine materials, Int. J. Mach. Tool Manu. 170 (2021), https://doi.org/10.1016/j.ijmachtools.2021.103804.
[3] A. Rutecka, M. Kursa, K. Pietrzak, K. Kowalczyk-Gajewska, K. Makowska, M. Wyszkowski, Damage evolution in AA2124/SiC metal matrix composites under

tension with consecutive unloadings, Archives of Civil and Mechanical Engineering 20 (2020) 1–18, https://doi.org/10.1007/s43452-020-00134-x.
[4] S. Kannan, H.A. Kishawy, Tribological aspects of machining aluminium metal matrix composites, J. Mater. Process. Technol. 198 (2008) 399–406, https://doi.org/10.1016/j.jmatprotec.2007.07.021.
[5] J. Liu, J. Li, C. Xu, Interaction of the cutting tools and the ceramic-reinforced metal matrix composites during micro-machining: A review, CIRP J. Manuf. Sci. Technol. 7 (2014) 55–70, https://doi.org/10.1016/j.cirpj.2014.01.003.
[6] S. Guo, S. Lu, B. Zhang, C.F. Cheung, Surface integrity and material removal mechanisms in high-speed grinding of Al/SiCp metal matrix composites, Int. J. Mach. Tool Manu. 178 (2022), https://doi.org/10.1016/j.ijmachtools.2022.103906.
[7] K. Lin, S.D. Pang, The influence of thermal residual stresses and thermal generated dislocation on the mechanical response of particulate-reinforced metal matrix nanocomposites, Compos. B Eng. 83 (2015) 105–116, https://doi.org/10.1016/j.compositesb.2015.08.008.
[8] A. Arun Premnath, Studies on machining parameters while milling particle reinforced hybrid (Al6061/Al2O3/Gr) MMC, Part. Sci. Technol. 33 (2015) 682–692, https://doi.org/10.1080/02726351.2015.1025457.
[9] O. Gavalda Diaz, D.A. Axinte, Towards understanding the cutting and fracture mechanism in Ceramic Matrix Composites, Int. J. Mach. Tool Manu. 118–119 (2017) 12–25, https://doi.org/10.1016/j.ijmachtools.2017.03.008.
[10] M.D. Hayat, H. Singh, Z. He, P. Cao, Titanium metal matrix composites: An overview, Compos. A Appl. Sci. Manuf. 121 (2019) 418–438, https://doi.org/10.1016/j.compositesa.2019.04.005.
[11] P.J. Doorbar, S. Kyle-Henney, Development of continuously-reinforced metal matrix composites for aerospace applications, Elsevier Ltd. (2017), https://doi.org/10.1016/B978-0-12-803581-8.09983-5.
[12] C. Wang, G. Liu, Q. An, M. Chen, Occurrence and formation mechanism of surface cavity defects during orthogonal milling of CFRP laminates, Compos. B Eng. 109 (2017) 10–22, https://doi.org/10.1016/j.compositesb.2016.10.015.
[13] S. Qingliang, W. Tiyuan, S. Qiang, Y. Fang, L. Hejun, M.W. Fu, Unraveling of the laser drilling of carbon/carbon composites: Ablation mechanisms, shape evolution, and damage evaluation, Int. J. Mach. Tool Manu. 184 (2023), https://doi.org/10.1016/j.ijmachtools.2022.103978.
[14] H. Chen, W. Zhu, H. Tang, W. Yan, Oriented structure of short fiber reinforced polymer composites processed by selective laser sintering: The role of powder-spreading process, Int. J. Mach. Tool Manu. 163 (2021), https://doi.org/10.1016/j.ijmachtools.2021.103703.
[15] S. Zan, Z. Liao, J.A. Robles-Linares, G. Garcia Luna, D. Axinte, Machining of long ceramic fibre reinforced metal matrix composites – How could temperature influence the cutting mechanisms? Int. J. Mach. Tool Manu. 185 (2023), 103994 https://doi.org/10.1016/j.ijmachtools.2023.103994.
[16] A. la Monaca, J.W. Murray, Z. Liao, A. Speidel, J.A. Robles-Linares, D.A. Axinte, M. C. Hardy, A.T. Clare, Surface integrity in metal machining - Part II: Functional performance, Int. J. Mach. Tool Manu. 164 (2021), https://doi.org/10.1016/j.ijmachtools.2021.103718.
[17] K.M. Rahman, V.A. Vorontsov, S.M. Flitcroft, D. Dye, A High Strength Ti–SiC Metal Matrix Composite, Adv. Eng. Mater. 19 (2017), https://doi.org/10.1002/adem.201700027.
[18] Y. Wang, X. Xu, W. Zhao, N. Li, S.A. McDonald, Y. Chai, M. Atkinson, K.J. Dobson, S. Michalik, Y. Fan, P.J. Withers, X. Zhou, T.L. Burnett, Damage accumulation during high temperature fatigue of Ti/SiCf metal matrix composites under different stress amplitudes, Acta Mater. 213 (2021), https://doi.org/10.1016/j.actamat.2021.116976.
[19] A. Manna, B. Bhattacharyya, A study on different tooling systems during machining of Al/SiC-MMC, J. Mater. Process. Technol. 123 (2002) 476–482, https://doi.org/10.1016/S0924-0136(02)00127-9.
[20] J. Sheikh-Ahmad, J.P. Davim, Tool wear in machining processes for composites, Machining Technology for Composite Materials. (2012) 116–153. doi: 10.1533/9780857095145.1.116.
[21] T.H.S. Mohamed, I.A. Azwan, S.A.M. Mohd, R.M.J. Mohd, S. Naheed, Machining and Machinability of Fiber Reinforced Polymer Composites, Springer Singapore (2021), https://doi.org/10.1007/978-981-33-4153-1.
[22] R. Hussein, A. Sadek, M.A. Elbestawi, M.H. Attia, An investigation into tool wear and hole quality during low-frequency vibration-assisted drilling of CFRP/Ti6Al4V stack, Journal of Manufacturing and Materials Processing. 3 (2019), https://doi.org/10.3390/jmmp3030063.
[23] S.A. Niknam, S. Kamalizadeh, A. Asgari, M. Balazinski, Turning titanium metal matrix composites (Ti-MMCs) with carbide and CBN inserts, Int. J. Adv. Manuf. Technol. 97 (2018) 253–265, https://doi.org/10.1007/s00170-018-1926-9.
[24] B. Wang, Z. Liu, Y. Cai, X. Luo, H. Ma, Q. Song, Z. Xiong, Advancements in material removal mechanism and surface integrity of high speed metal cutting: A review, Int. J. Mach. Tool Manu. 166 (2021), https://doi.org/10.1016/j.ijmachtools.2021.103744.
[25] I. Shyha, D. Huo, Introduction-Engineering Materials Advances in Machining of Composite Materials Conventional and Non-conventional Processes, 2021.
[26] G. Li, M.Z. Rahim, W. Pan, C. Wen, S. Ding, The manufacturing and the application of polycrystalline diamond tools – A comprehensive review, J. Manuf. Process. 56 (2020) 400–416, https://doi.org/10.1016/j.jmapro.2020.05.010.
[27] M. Wang, Z. Zheng, Z. Wu, J. Zhang, X. Chen, J. Xiao, J. Xu, Investigation on the machinability of SiCp/Al composite by in-situ laser assisted diamond cutting, J. Mater. Process. Technol. 318 (2023), 118044, https://doi.org/10.1016/j.jmatprotec.2023.118044.
[28] G. Chryssolouris, N. Anifantis, S. Karagiannis, Laser assisted machining: An overview, J. Manuf. Sci. E. T. ASME 119 (1997) 766–769, https://doi.org/10.1115/1.2836822.
[29] K. You, F. Fang, G. Yan, Surface generation of tungsten carbide in laser-assisted diamond turning, Int. J. Mach. Tool Manu. 168 (2021), https://doi.org/10.1016/j.ijmachtools.2021.103770.
[30] Z. Shang, Z. Liao, J.A. Sarasua, J. Billingham, D. Axinte, On modelling of laser assisted machining: Forward and inverse problems for heat placement control, Int. J. Mach. Tool Manu. 138 (2019) 36–50, https://doi.org/10.1016/j.ijmachtools.2018.12.001.
[31] K. You, G. Yan, X. Luo, M.D. Gilchrist, F. Fang, Advances in laser assisted machining of hard and brittle materials, J. Manuf. Process. 58 (2020) 677–692, https://doi.org/10.1016/j.jmapro.2020.08.034.
[32] D. Xu, Z. Liao, D. Axinte, J.A. Sarasua, R. M'Saoubi, A. Wretland, Investigation of surface integrity in laser-assisted machining of nickel based superalloy, Mater. Des. 194 (2020), https://doi.org/10.1016/j.matdes.2020.108851.
[33] C. Ni, L. Zhu, Z. Zheng, J. Zhang, Y. Yang, R. Hong, Y. Bai, W.F. Lu, H. Wang, Effects of machining surface and laser beam scanning strategy on machinability of selective laser melted Ti6Al4V alloy in milling, Mater. Des. 194 (2020), https://doi.org/10.1016/j.matdes.2020.108880.
[34] S.K. Nandi, R. Kumar, A. Agrawal, Computationally inexpensive semi-analytical thermal model to predict melt-pool dimensions for a single-track in Selective Laser Melting, J. Manuf. Process. 80 (2022) 469–479, https://doi.org/10.1016/j.jmapro.2022.06.025.
[35] N.T. Nguyen, A. Ohta, K. Matsuoka, N. Suzuki, Y. Maeda, Analytical Solutions for Transient Temperature of Semi-Infinite Body Subjected to 3-D Moving Heat Sources, Welding Journal (miami, Fla) 78 (1999).
[36] I. Mendoza, D. Villalobos, B.T. Alexandrov, Crack propagation of Ti alloy via adiabatic shear bands, Mater. Sci. Eng. A 645 (2015) 306–310, https://doi.org/10.1016/j.msea.2015.08.035.
[37] R. Pederson, Microstructure and Phase Transformation of Ti-6Al-4V, 2002.
[38] X. Li, X. Liu, C. Yue, S.Y. Liang, L. Wang, Systematic review on tool breakage monitoring techniques in machining operations, Int. J. Mach. Tool Manu. 176 (2022), https://doi.org/10.1016/j.ijmachtools.2022.103882.
[39] B. Toubhans, G. Fromentin, F. Viprey, H. Karaouni, T. Dorlin, Machinability of inconel 718 during turning: Cutting force model considering tool wear, influence on surface integrity, J. Mater. Process. Technol. 285 (2020), 116809, https://doi.org/10.1016/j.jmatprotec.2020.116809.
[40] Y. Su, L. Li, G. Wang, Machinability performance and mechanism in milling of additive manufactured Ti6Al4V with polycrystalline diamond tool, J. Manuf. Process. 75 (2022) 1153–1161, https://doi.org/10.1016/j.jmapro.2022.01.065.
[41] T. Childerhouse, R. M'Saoubi, L.F.P. Franca, P. Crawforth, M. Jackson, Machining performance and wear behaviour of polycrystalline diamond and coated carbide tools during milling of titanium alloy Ti-54M, Wear 523 (2023), 204791, https://doi.org/10.1016/j.wear.2023.204791.
[42] B. Deng, F. Peng, L. Zhou, H. Wang, M. Yang, R. Yan, A comprehensive study on flank wear progression of polycrystalline diamond micro-tool during micro end-milling of SiCp/Al composites, Wear 456–457 (2020), 203291, https://doi.org/10.1016/j.wear.2020.203291.
[43] Y. Feng, T.P. Hung, Y.T. Lu, Y.F. Lin, F.C. Hsu, C.F. Lin, Y.C. Lu, S.Y. Liang, Flank tool wear prediction of laser-assisted milling, J. Manuf. Process. 43 (2019) 292–299, https://doi.org/10.1016/j.jmapro.2019.05.008.
[44] K. Zhou, J. Xu, G. Xiao, Y. Huang, A novel low-damage and low-abrasive wear processing method of Cf/SiC ceramic matrix composites: Laser-induced ablation-assisted grinding, J. Mater. Process. Technol. 302 (2022), 117503, https://doi.org/10.1016/j.jmatprotec.2022.117503.
[45] D.T. Blagoeva, J.B.J. Hegeman, M. Jong, M.C.R. Heijna, S.M. Gonzalez de Vicente, T. Bakker, P. ten Pierick, H. Nolles, Characterisation of 2D and 3D Tyranno SA 3 CVI SiCf/SiC composites, Mater. Sci. Eng. A 638 (2015) 305–313, https://doi.org/10.1016/j.msea.2015.04.090.
[46] D. Axinte, H. Huang, J. Yan, Z. Liao, What micro-mechanical testing can reveal about machining processes, Int. J. Mach. Tool Manu. 183 (2022), https://doi.org/10.1016/j.ijmachtools.2022.103964.
[47] K. Palaniappan, M. Sundararaman, H. Murthy, R. Jeyaraam, B.C. Rao, Influence of workpiece texture and strain hardening on chip formation during machining of Ti–6Al–4V alloy, Int. J. Mach. Tool Manu. 173 (2022), https://doi.org/10.1016/j.ijmachtools.2021.103849.
[48] N.H. Cook, P. Jhaveri, N. Nayak, The mechanism of chip curl and its importance in metal cutting, J. Manuf. Sci. E. T. ASME 85 (1963) 374–380, https://doi.org/10.1115/1.3669898.
[49] B. Worthington, A.H. Redford, Chip curl and the action of the groove type chip former, International Journal of Machine Tool Design and Research. 13 (1973) 257–270, https://doi.org/10.1016/0020-7357(73)90004-8.
[50] M. Wu, A. Yu, Q. Chen, Y. Wang, J. Yuan, L. Sun, J. Chi, Design of adjustable chip breaker for PCD turning tools, Int. J. Mech. Sci. 172 (2020), https://doi.org/10.1016/j.ijmecsci.2019.105411.
[51] B. Yılmaz, Ş. Karabulut, A. Güllü, Performance analysis of new external chip breaker for efficient machining of Inconel 718 and optimization of the cutting parameters, J. Manuf. Process. 32 (2018) 553–563, https://doi.org/10.1016/j.jmapro.2018.03.025.